

A Closer Look at Benchmarking Self-Supervised Pre-training with Image Classification

Markus Marks^{*1}, Manuel Knott^{*1,2,3,4}, Neehar Kondapaneni¹, Elijah Cole^{1,5},
Thijs Defraeye⁴, Fernando Perez-Cruz^{2,3,6}, and Pietro Perona¹

¹California Institute of Technology

²ETH Zurich, Institute for Machine Learning, Department of Computer Science

³Swiss Data Science Center, ETH Zurich and EPFL

⁴Empa, Swiss Federal Laboratories for Materials Science and Technology

⁵Altos Labs

⁶Bank for International Settlements (BIS)

Abstract

Self-supervised learning (SSL) is a machine learning approach where the data itself provides supervision, eliminating the need for external labels. The model is forced to learn about the data's inherent structure or context by solving a pretext task. With SSL, models can learn from abundant and cheap unlabeled data, significantly reducing the cost of training models where labels are expensive or inaccessible. In Computer Vision, SSL is widely used as pre-training followed by a downstream task, such as supervised transfer, few-shot learning on smaller labeled data sets, and/or unsupervised clustering. Unfortunately, it is infeasible to evaluate SSL methods on all possible downstream tasks and objectively measure the quality of the learned representation. Instead, SSL methods are evaluated using in-domain evaluation protocols, such as fine-tuning, linear probing, and k-nearest neighbors (kNN). However, it is not well understood how well these evaluation protocols estimate the representation quality of a pre-trained model for different downstream tasks under different conditions, such as dataset, metric, and model architecture. In this work, we study how classification-based evaluation protocols for SSL correlate and how well they predict downstream performance on different dataset types. Our study includes eleven common image datasets and 26 models that were pre-trained with different SSL methods or have different model backbones. We find that in-domain linear/kNN probing protocols are, on average, the best general predictors for out-of-domain performance. We further investigate the importance of batch normalization for the various protocols and evaluate how robust correlations are for different kinds of dataset domain shifts. In addition, we challenge assumptions about the relationship between discriminative and generative self-supervised methods, finding that most of their performance differences can be explained by changes to model backbones.

1 Introduction

There has been a trend in machine learning where algorithmic improvements follow challenges posed through new datasets and evaluation metrics. How we evaluate new ML methods is therefore crucial, as the community may optimize for flawed [1] or misleading [2] metrics. Self-supervised learning (SSL) is a promising path to advance machine learning using unlabeled data. It describes techniques that enable learning general image representations from abundant and cheap unlabeled data by solving pretext tasks [3]. Because of its effectiveness, SSL in computer vision has been used in a wide array of domains, ranging from animal behavior [4], retinal disease detection [5], computational histopathology [6] to remote sensing [7]. SSL has proven more robust to data distribution shifts than supervised learning [8]. Fundamentally, SSL methods aim to

^{*}Equal contribution.

Code available at: https://github.com/manuelknott/ssl_eval_protocols

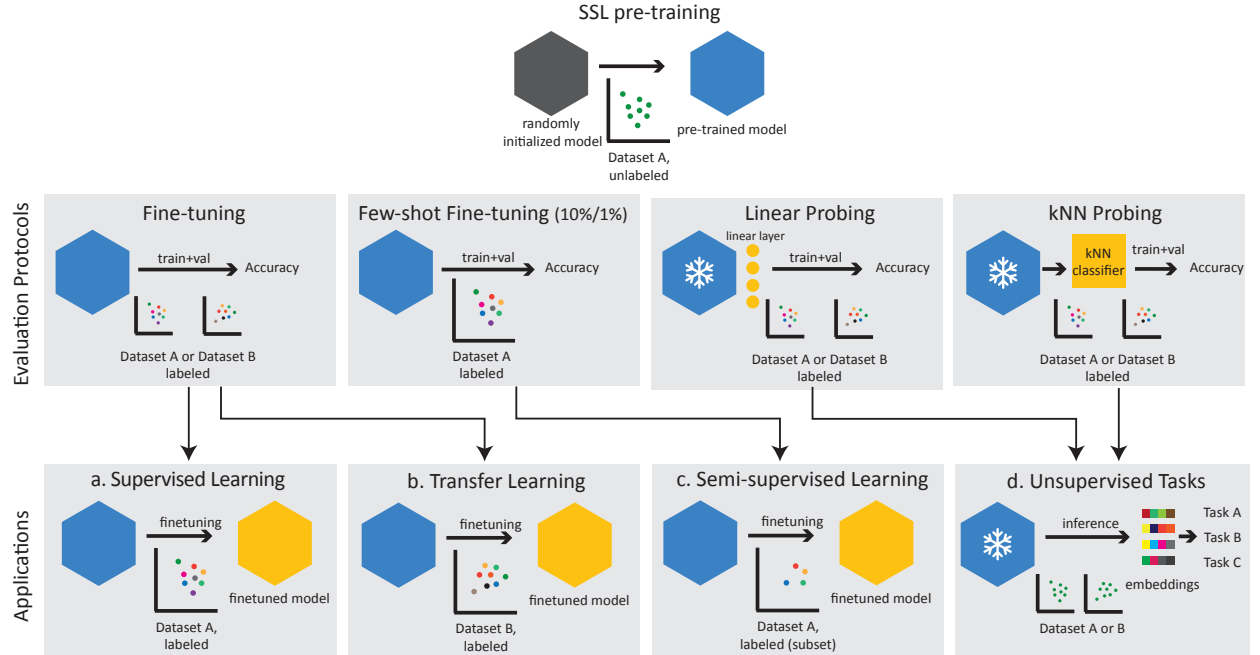


Figure 1: SSL application scenarios: We illustrate the following applications of self-supervised learning: a) supervised learning (training and fine-tuning on the same dataset), b) transfer learning (train on a large dataset and fine-tune the model on a —usually smaller—domain dataset), c) semi-supervised learning (train on a large unlabeled dataset and fine-tune on a small labeled subset of it), d) unsupervised tasks (train on a dataset and run inference with the resulting model on any dataset to create embeddings that can be used for downstream tasks other than classification). Arrows between protocols and applications indicate a direct relationship.

learn a general representation useful for *any* downstream task. What is “downstream task performance” and how should it be measured? We first consider the different applications of self-supervised pre-training. Fig. 1 (bottom) depicts the main practical applications where self-supervised pre-training is applied:

- Supervised Learning:* A model is pre-trained on dataset A via SSL and then fine-tuned on the same dataset in a supervised way. This procedure can yield higher overall accuracies than supervised training from randomly initialized model weights [9, 10].
- Transfer Learning:* A model is pre-trained on dataset A via SSL. The pre-trained backbone is then fine-tuned on a typically smaller labeled domain dataset B . This classical transfer learning paradigm can achieve better results with fewer data on small domain-specific data sets [11]. SSL is usually a better starting point for transfer learning compared to supervised pre-training [8], as the latter is prone to overfit on features that are only useful for solving the initial supervised task [12].
- Semi-supervised Learning*¹: A model is pre-trained on an unlabelled dataset A via SSL, followed by supervised fine-tuning on a small and labeled subset of the same dataset. This is particularly useful when data is cheap but labeling is expensive. [13, 14, 16, 17]
- Unsupervised Tasks/Clustering:* A model is pre-trained on dataset A via SSL. It is then used to generate embeddings at inference time. These embeddings can be used for various downstream tasks without further training the model [4, 18, 19].

¹The term *semi-supervised learning* is commonly used to describe the “self-supervised pretrain, supervised fine-tune on a subset” paradigm (see e.g., [13–15]). We adopt this usage but acknowledge that, originally, semi-supervised learning refers to methods that utilize labeled and unlabeled data simultaneously rather than sequentially.

Evaluating the performance of SSL methods is challenging since there are endless ways to evaluate their learned representations, and exploring all of them is impossible. The community has developed several evaluation protocols to compare the representations’ quality, resulting in *proxy metrics* for unobserved downstream tasks. Many of these protocols use the learned representation to solve classification tasks, for example, through linear probing, end-to-end fine-tuning, or by evaluating the embedding representation with a kNN classifier. The similarities and differences in the expressiveness of various protocols are understudied, which leads to an inconsistent evaluation and comparison of SSL methods (see Appendix A). In this work, we show how reliably different protocols rank SSL methods w.r.t. to their performance on different downstream tasks. In detail, our contributions are as follows:

- We survey existing papers on self-supervised learning methods for images and provide a structured summary of established evaluation protocols.
- We correlate in-domain (ID) and out-of-domain (OOD) top-1 and top-5 classification accuracies obtained from fine-tuning, linear probing, and kNN probing on 26 SSL-pretrained models. We show that linear/kNN probing protocols yield the proxy metrics that can, on average, best predict the *ranking* of SSL methods on eleven OOD datasets.
- We explore two kinds of domain shifts—categorical shift (either with coarse-grained or fine-grained features) and style shift—and find that in-domain proxy metrics vary in their predictiveness for each type of domain shift.
- We compare generative and discriminative SSL protocols for ResNet and ViT backbones. We find that relative differences in linear probing and fine-tuning performance are more due to backbone architecture than the SSL family.

2 Related Work

2.1 Self-Supervised Learning

Self-supervised learning plays a crucial role in the recent success of natural language processing models [20, 21] and computer vision [9, 14, 17, 22] and finds applications in tasks like speech recognition [23], video classification [24], point cloud reconstruction [25] or behavioral analysis [4]. SSL relies on designing pretext tasks, forcing the model to learn a functional representation of the data without providing external labels [3]. Most SSL algorithms for images fall into one of two major categories: *discriminative* and *generative* methods [26].

Discriminative methods. Contrastive SSL methods for vision generate augmentations of samples and discriminate them from other samples in the data set [14, 27]. These methods rely on negative samples and, therefore, require large batch sizes. A second line of work (*self-distillation*) solely relies on positive samples [16, 28]. Yet another group of *clustering-based* methods utilizes pseudo-labels based on k-means clustering in order to learn image representations [29, 30].

Generative methods. Transformers [31] are the current state-of-the-art deep-neural network architecture across many AI fields, bridging language and vision models. Inspired by pretext tasks for language transformer models, such as masking in BERT [9, 21] recently introduced masked auto-encoding for images, an effective pre-training method, by which an image is split into patches, and about 70 percent of the patches are masked. Based on the remaining patches, the transformer will reconstruct the masked patches. MaskFeat [32] showed that the use of HOG features [33] as reconstruction targets of masked patches is an effective pretext task. Recent work combines masked image modeling with language-guided representations [34, 35]. Another approach focuses on pixel-level reconstruction, alleviating the problem of missing foreground information that can occur with patch-based reconstruction approaches [36].

2.2 SSL Evaluation Protocols

In general, self-supervised pre-training aims to learn useful representations across various downstream tasks. However, the quality of representations varies depending on the task. For example, some tasks may require representations invariant to certain transformations, while others may require representations preserving fine-grained details. For those reasons, designing evaluation protocols and associated metrics that capture all aspects is challenging. We conducted a literature survey on the different evaluation metrics used in SSL papers (Appendix A). This section gives an overview of the most popular evaluation metrics. Typically, a study uses a set of a few metrics to evaluate the performance. This study mainly focuses on classification-based protocols, for which we identified four variations described in more detail below. Fig. 1 illustrates their relationship to the previously mentioned use cases.

K-nearest neighbors (kNN). kNN-classification is a way of probing the model, assuming that similar samples should have close Euclidean proximity in the latent space (see, e.g., [17, 22, 28, 37]). Compared to linear probing, kNN classifiers are fast and computationally light to deploy, often without an iterative learning setup [22]. Since kNN requires no training, one could argue that this is the most direct and cheapest evaluation for representation learning. However, clustering in high-dimensional spaces can be challenging [38]. Another issue is that different dimensions do not necessarily have the same scale and might need to be normalized.

Linear probing. In most cases, the classifier is implemented as a logistic regression model via a single fully-connected layer, usually referred to as *Linear Probing* (see, e.g., [9, 10, 14–17, 22, 39–43]). The intuition here is that the learned representation is good if the dataset classes (the model was not trained on) are linearly separable. Besides linear and kNN probing, researchers sometimes use other shallow classifiers, e.g., Support Vector Machines [28, 37, 44–46].

End-to-end fine-tuning. Like linear probing, the end-to-end fine-tuning protocol replaces the last layer of a model with a linear classifier. In this setting, all model parameters are trained, allowing latent representations to adapt to the supervised task and/or a new data set (see, e.g., [9, 10, 14, 15, 17, 32, 35, 40, 47]). Some papers use a partial fine-tuning protocol where only parts of the model are trained [9, 48, 49].

Few-shot fine-tuning. The few-shot learning protocol follows the same procedure as end-to-end fine-tuning but only uses a subset of the available training labels (typically 10% or 1%) (see, e.g., [14, 16, 17, 28, 43]), which makes evaluation significantly more efficient.

Some common protocols that do not use classification are not included in the experimental part of this study but should be mentioned at this point. Our survey found that task transfer protocols, such as object detection [9, 15, 17, 28, 39, 41], semantic segmentation [9, 10, 15–17], depth estimation [16], copy detection [22], image retrieval [22], and super-resolution [10], are frequently used to benchmark SSL methods. Less commonly, unsupervised clustering, e.g., k-means, is used in the context of SSL evaluation (see, e.g., [17, 50]).

2.3 Studies on SSL Evaluation Protocols

While the community focuses on improving the capacity of SSL methods, evaluation protocols are seldom challenged. However, some studies can be used as references.

Kim et al. [51] compared self-supervised and supervised pre-training for domain transfer. They evaluated fine-tuning accuracy on four downstream datasets for models pre-trained either supervised on ImageNet or SSL. By comparing four SSL methods, they found that supervised pre-training consistently outperformed SSL regarding OOD fine-tuning accuracy. As a shortcoming of their study, they mention the lack of possible combinations of different backbones with different SSL methods, which we address in our study.

Yang et al. [52] define an OOD benchmark for large language models. They find that distribution shifts between ID and OOD dominate OOD generalization results for language. They find discriminative models show a stronger linear correlation between ID and OOD performance than generative models. They find

that linear probing shows relatively low ID and OOD accuracy, differing from findings in computer vision, where Kumar et al. [53] find that FT can do worse than LP for large distribution shifts.

Newell and Deng [54] find that the performance of an SSL algorithm in one setting might not translate to another. Moreover, they see that LP performance does not correlate with FT performance. Linear transferability occurs when data from the same class in different domains are more related to each other than data from other classes in different domains [55].

Ibrahim et al. [56] measure the robustness of SOTA vision models, including SSL models, against distribution shifts w.r.t. factors of variation such as background, pose, etc., and find that the learning objective is more impactful for robustness than architecture. Other studies have focused on understanding optimal SSL methods in the context of various metrics on ImageNet, such as fine-tuning accuracy, linear probing, and k-nearest neighbors [57, 58].

Miller et al. [59] ask whether accuracy depends on in-domain to out-of-domain distributions shift, i.e. training on CIFAR-10 [60] and testing on CIFAR-10.1 [61]. They find that the linear trend between in-domain and out-of-domain performance holds across many but not all datasets.

Cole et al. [62] explore challenges in generalizing contrastive self-supervised learning beyond ImageNet, finding limitations with respect to data quantity, domain transfer, robustness, and fine-grained task performance.

Recently, Goldblum et al. [63] compared a wide range of architectural backbones and SSL setups on multiple datasets and downstream tasks. They focus on finding the backbone and method that generalizes best. In contrast, our research focuses on which metric to use when developing SSL methods. Our findings challenge the wide use of fine-tuning as a metric [9, 24, 32], as it does not strongly predict performance across different tasks and metrics.

Liu et al. [26] conducted a comparative study between discriminative and generative SSL methods among several domains (not limited to vision). They claim that contrastive learning methods—MoCo and SimCLR in particular—are effective if the downstream task is classification, while this is not obvious for many generation tasks.

While some work has compared discriminative and generative models’ influence on performance in vision [10, 32, 64], our study posits that the backbone of the model has more impact on performance than pre-training or pretext tasks. Specifically, we compare Vision Transformers (ViTs) with Residual Networks (ResNets), both indirectly and directly.

A recent study [65] presents a motivation akin to ours. However, the scope of our study is considerably larger as we compare more models (26 compared to 7), more OOD datasets (11 compared to 4), and a broader range of evaluation protocols, including three distinct fine-tuning protocols (100%, 10%, and 1%). Additionally, our study evaluates various model architectures, contrasting ResNets with Vision Transformers, and explores different types of domain shifts—categorical and style—by selecting transfer learning datasets.

3 Experimental Setup

Models and protocols. Our experiments are based on pre-trained models published by the original authors (if available) or replicas that achieve similar results to those reported in the original papers (see Appendix E for sources of the pre-trained model weights). We use ResNet-50 and ViT-B16 backbones in this study. All models were pre-trained on ImageNet-1k [66]. We measure the accuracies of an SSL method on its training dataset (ImageNet) using five evaluation protocols: linear probing, kNN probing, and three variations of end-to-end fine-tuning with 100%, 10%, or 1% of the available training data (see Fig. 1, top). In addition, we compute kNN, linear probing, and fine-tuning (100%) metrics on multiple OOD datasets for each SSL method.

Correlation analysis. We spearman-correlate the results of the different protocols across 26 different SSL methods. Linear and kNN probing are evaluated with and without normalizing the embedding. We found that normalization has no significant effect on some models and a large positive effect on others, especially those using masked image modeling. This aligns with findings from previous research [65]. All LP and kNN results reported in the main part of this paper use the normalized version (non-normalized results are reported in the supplementary materials).

OOD Datasets. For domain-shift analyses, we select our datasets following insights from previous work. It has been shown that the performance of current SSL models depends on the granularity of the dataset classes [62]. We, therefore, choose datasets of different granularities in our study. We chose Caltech-256 [67], Pascal VOC 2012 [68], and iNaturalist 2021 mini [69] (“Family” target) as representative datasets with coarse-grained classes. In addition, we evaluate CUB [70] and two more variations of iNaturalist 2021 mini—with “Genus” or “Species” as target classes—as fine-grained datasets (see Appendix D for details on how the iNaturalist datasets are constructed). We also compare categorical domain shift and stylistic domain shift with respect to ImageNet. We group all previously mentioned datasets, excluding Pascal VOC, to create a group with no or few shared categories with ImageNet. This group is our categorical domain shift group. We use the ImageNet-D [71] dataset (ImageNet vocabulary but different styles) for stylistic domain shifts. A tabular overview of the dataset assignment described in this paragraph can be found in Tab. S.6.

Hyperparameter selection. Usually, researchers sweep over a set of different hyperparameters during pre-training to find the best configuration for their method and evaluation protocols. This results in a variety of different hyperparameters for the same protocol. Therefore, it is very difficult to directly compare the reported metrics as they are confounded by the different choices of hyperparameters. We decided to standardize our protocols by finding “typical” hyperparameter configurations for each of the protocols derived from the literature and use them for all models (see Appendix E for implementation details). Consequently, the metrics we found in our experiments may deviate from the ones reported by the original authors. However, this standardization is crucial as our goal is not to benchmark the overall performance of different SSL methods but to correlate evaluation metrics under comparable conditions.

Robustness. In order to quantify variance introduced by random seeding, we calculate means and standard deviations for one model per protocol and dataset and repeat the same experiments for this selection three times (see Appendix F).

4 Results

4.1 Which in-domain metric best predicts out-of-domain rankings on average?

We begin our analysis by visualizing the rank correlations averaged across all models and datasets. In Fig. 2, left panel, we see the ID metrics correlated against themselves. Expectedly, ID metrics generally correlate highly, with linear probing and 10%-fine-tuning having the highest ($r = 0.90$, $r = 0.91$) and fine-tuning having the lowest average correlation coefficient ($r = 0.79$). Notably, Linear and kNN probing correlate almost perfectly ($r = 0.99$) when features are normalized (Fig. 2). When comparing ID with OOD metrics, correlation coefficients are visibly lower, indicating that domain shifts affect both the absolute accuracy and also the ranking of different SSL representations. We will further investigate these effects in Sec. 4.2.

Next, we target the question of whether an ID metric on training data is a good proxy metric for OOD use cases. We consider two use cases: (1) transfer learning, expressed by OOD fine-tuning accuracies averaged over multiple datasets, and (2) unsupervised representation learning, expressed by OOD kNN and/or linear probing accuracies averaged over multiple datasets. We can observe that the probing protocols (kNN and linear) correlate most with themselves and each other when comparing ID and OOD accuracies. Overall, linear probing is the best OOD predictor when averaged across metrics and datasets ($r = 0.85$), followed closely by kNN ($r = 0.84$). Interestingly, the two few-shot protocols appear to be the best predictors of model performance for out-of-distribution (OOD) fine-tuning. This correlation may arise from two primary factors: First, batch normalization on the embeddings is applied during the probing protocols but not for fine-tuning, which we discuss in more detail in Sec. 4.3. Second, the transfer learning datasets in our study contain fewer training samples compared to ImageNet, resulting in a number of training steps during OOD fine-tuning that more closely resembles those in the few-shot in-distribution (ID) protocols rather than those used for fine-tuning on the full ImageNet dataset.

Summary: While probing protocols are the best OOD predictors on average, one should rely on few-shot fine-tuning (10%) to predict the transfer learning capability for OOD fine-tuning.

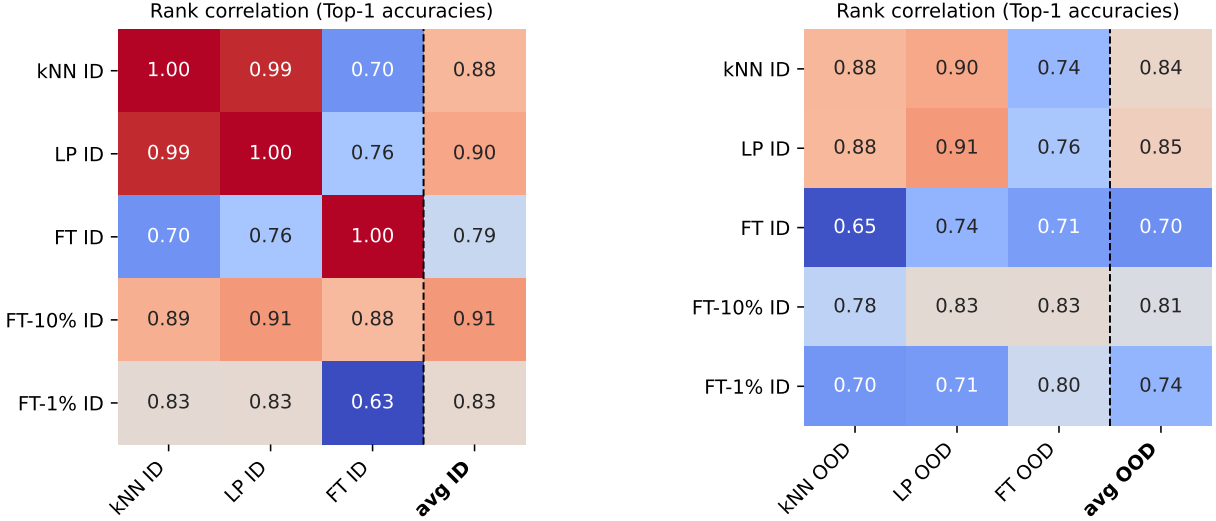


Figure 2: Comparing Spearman rank correlations of top-1 classification accuracies obtained by different evaluation protocols (kNN: k-nearest neighbors, LP: linear probing, FT: fine-tuning, FT-10%: 10%-fine-tuning, FT-1%: 1%-fine-tuning). In-domain (ID) refers to ImageNet-1k, which was also used for pre-training. Out-of-domain (OOD) metrics are averaged over eleven datasets as described in Sec. 3. In-domain metrics generally correlate highly (left panel), with fine-tuning having the weakest average correlation coefficient. When comparing ID with OOD protocols (right panel), correlation coefficients are visibly lower, indicating a domain-shift effect that impacts the absolute accuracy and the protocols’ rank ordering (correlation). A more verbose version of these matrices showing additional protocol variations (with and without feature normalization) is shown in Fig. S.3.

4.2 How do protocols differ under different kinds of domain shift?

Fig. 3 assesses the average rank correlations of top-1 accuracies under the four described domain shifts. In each panel, we explore the rank correlation of each in-domain metric against a single OOD metric averaged over domain shift grouped datasets. Generally, when comparing ID metrics with OOD metrics, we observe no notable difference between fine-grained and coarse-grained datasets but a significantly lower correlation for style-shift datasets.

OOD kNN. We can see that both ID probing protocols (kNN and linear) can reliably predict the ranking of OOD kNN accuracy for categorical domain shifts and less reliably for style-related domain shifts (left panel, top row). The correlation coefficient for categorical shift (kNN $r = 0.96$, LP $r = 0.95$) is notably higher than the equivalent for fine-tuning ($r = 0.62$).

OOD LP. The general pattern is similar to OOD kNN probing, with ID kNN and ID LP being the strongest predictors and style shifts having a stronger impact than categorical shifts. Few-shot fine-tuning protocols (1% and 10% correlate slightly more with OOD LP compared to OOD kNN).

OOD FT. In Fig. 2, ID FT is weakly correlated with OOD FT. In Fig. 3, we see that FT rankings are less predictable with respect to shifts in both category ($r = 0.73$) and style ($r = 0.61$). Surprisingly, in-domain probing (ID LP, ID kNN) and few-shot fine-tuning (ID FT-10% FT-1%) protocols are better correlated to OOD FT across all types of domain shifts. As these protocols are significantly cheaper than full end-to-end fine-tuning (see Tab. S.8 for the estimated computational costs of each ID protocol in our experiments), they can be used as a proxy for the ranking of OOD fine-tuning performance.

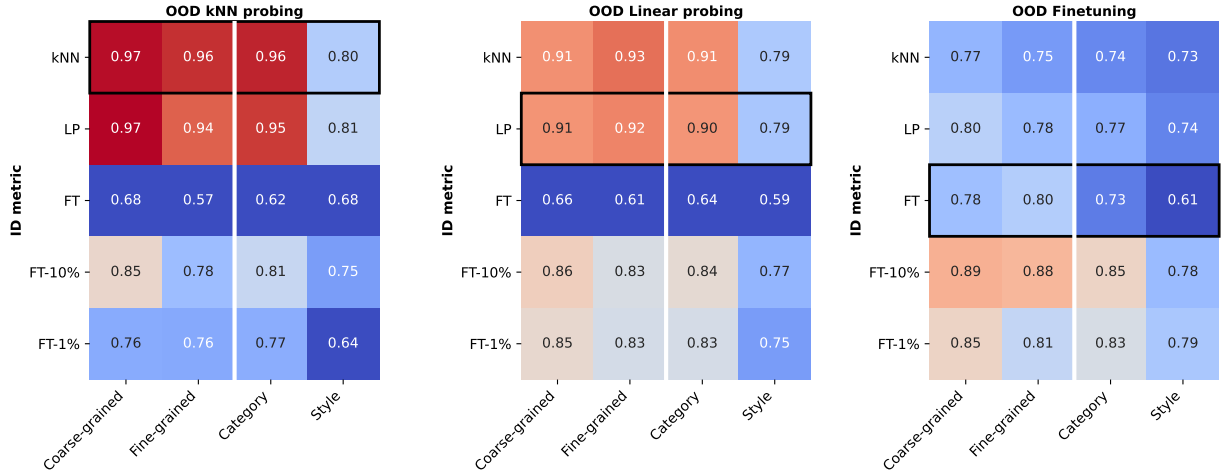


Figure 3: Spearman rank correlations of top-1 classification accuracies derived from in-domain and out-of-domain protocols under certain types of domain shift. We differentiate between fine-grained and coarse-grained categorical domain shifts (left half of each panel). Further, we compare categorical with stylistic domain-shift (right half of each panel). Black rectangles highlight when the same ID and OOD evaluation protocol is used.

Summary: The ranking of SSL methods is more robust for categorical and less for stylistic domain shifts under all protocols. There is no significant difference between fine-grained and coarse-grained categorical shifts.

4.3 What is the effect of embedding normalization on different protocols?

Previous research has pointed out the importance of embedding normalization for linear [9, 65] and kNN [65] probing. Our experiments confirm that using batch normalization before the final classification layer in linear probing and z-score normalization for kNN probing can significantly increase accuracy (see Tab. S.2). While the effect is strong for models with unscaled embedding representations (e.g., SimSiam and MaskFeat in our case), others (e.g., DINO) are neither positively nor negatively affected by normalization.

While batch normalization is common for linear probing, it is not established for fine-tuning protocols, presumably because feature scaling will be resolved during training when model weights are not frozen. We challenge this assumption and claim that this is only true if a model is trained long enough (e.g., 100 epochs on full ImageNet) while fine-tuning on smaller datasets or with fewer epochs can yield significantly higher accuracies when BatchNorm is applied. Fig. 4 displays fine-tuning accuracies with and without batch normalization for all the datasets included in our study, together with the total number of optimizer steps.

Summary: For models with unscaled features, batch normalization is critical for linear/kNN probing but also when fine-tuning on small datasets.

4.4 How do different SSL families and architectures perform under the various protocols?

Previous work hypothesized that generative SSL methods achieve higher fine-tuning accuracies through expressive but non-linear features [9]. Conversely, contrastive SSL methods achieve better linear probing performance through linearly separable features due to a discriminative loss function [32]. Following this hypothesis, recent studies have excluded linear probing altogether and have only used the fine-tuning protocol [24].

In Fig. 5, we plot the relation between each model’s fine-tuning and linear probing performance on ImageNet. We see that, indeed, the models with a generative loss (MaskFeat [32], MAE [9], BEiT v2 [72],

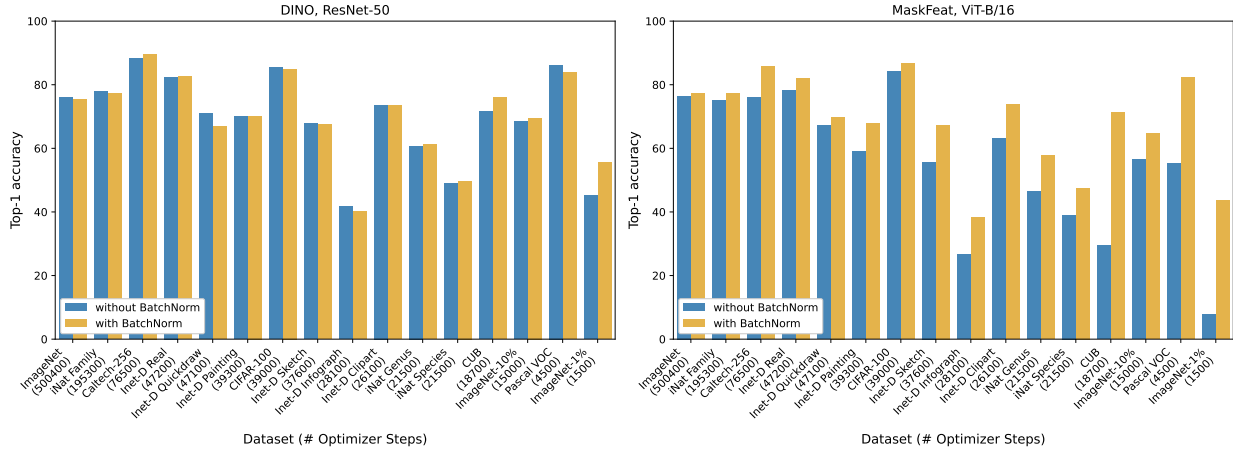


Figure 4: Fine-tuning accuracies with and without batch normalization for two exemplary models that appear to have scaled (left, DINO+ResNet-50) and unscaled (right, MaskFeat+ViT-B/16) embedding representations. The x-axes display all datasets included in this study and the number of optimizer steps derived from the dataset size, batch size, and total number of epochs. For MaskFeat, batch normalization has a significant effect when the number of optimizer steps is small and only a small effect when the number of steps is large, implying less-scaled features compared to DINO.

iBOT [17]) have a larger performance gap between fine-tuning and linear probing performance on ImageNet than discriminative models. However, generative methods have been introduced in more recent publications, and ViT backbones are frequently used instead of CNNs. Could this cause the relative difference between fine-tuning and linear-probing performance? The figure shows that ViT backbones are all above the regression line, indicating a higher fine-tuning accuracy relative to their linear probing accuracy compared to other models. We can more directly assess this effect using two SSL methods that use both the ResNet-50 and ViT-B/16 backbones (DINO and MoCo-v3). For these models, we see that switching to a ViT backbone moves them from below the regression line to above. This suggests that the relatively higher fine-tuning accuracy is caused by a difference in backbone architectures rather than the SSL family, which contrasts with previous hypotheses [9, 32]).

Summary: Differences in linear probing performance between generative and discriminative models can be explained through different backbones rather than SSL methods.

4.5 How do rank correlations relate to absolute performance?

Thus far, we have analyzed rank correlations between ID and OOD metrics. These correlations tell us how well the ranking of representations generated by an ID metric respects the ranking of the representations on the eleven OOD datasets we consider, and we have found several interesting trends. In Fig. 6, we show how these trends manifest in terms of absolute performance, in which we visualize OOD accuracy against ID accuracy under each of our three metrics. Whether OOD accuracy will be higher or lower than ID accuracy depends on several factors, such as the representation quality and the similarity of the target dataset compared to ImageNet. For certain datasets (e.g., CUB and iNat-mini), OOD performances can be significantly worse even though the method ranking is very similar. On three datasets, Pascal VOC, Caltech-256, and CUB, we see that kNN and linear probing have a more linear relationship between ID and OOD accuracy than fine-tuning. On these datasets, we can see that several SSL methods can have almost the same ID fine-tuning accuracy but significantly different OOD fine-tuning accuracy.

Summary: ID evaluation protocols can be robust proxies to estimate the ranking of SSL methods, but not their absolute performance.

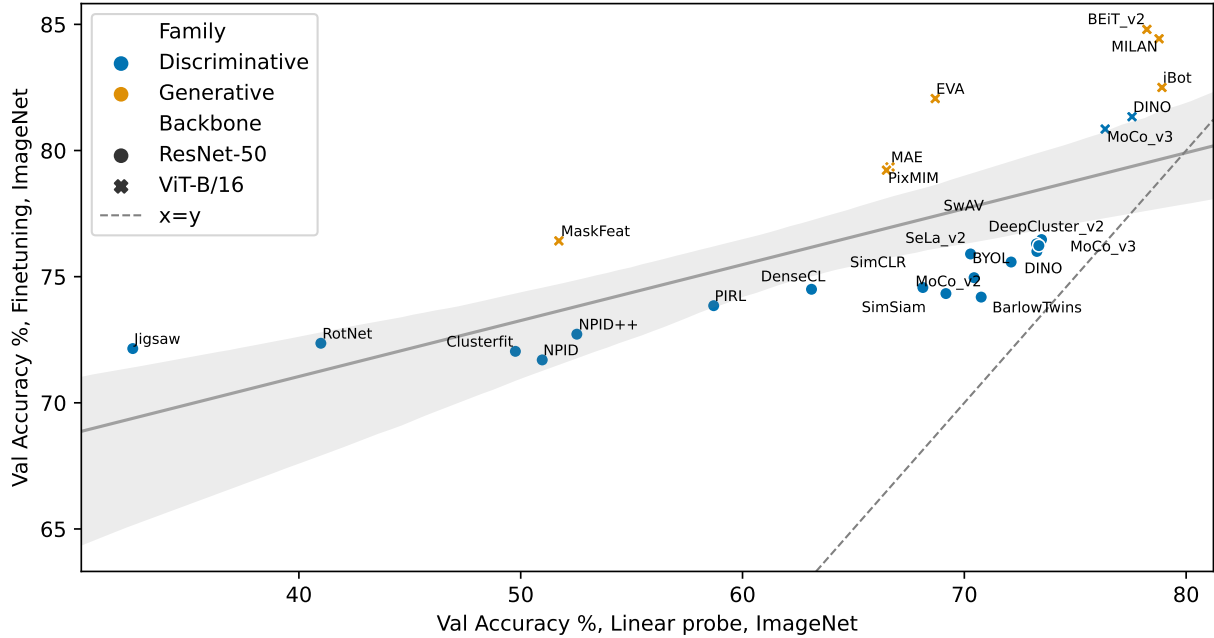


Figure 5: Scatter plot of the correlation of linear-probing and fine-tuning accuracies for ImageNet (in-domain). Each dot represents a model. The color codes for the model family, i.e., blue for discriminative and orange for generative models. Shapes indicate which backbones were used. The dotted line represents the equal error line; the solid line is a linear regression with a 90% confidence interval.

5 Discussion

Self-supervision is a powerful way of leveraging unlabeled data for further downstream tasks. Since the performance benchmark we choose will influence algorithmic development, it is crucial to evaluate SSL methods correctly for their intended purpose. However, SSL evaluation is non-trivial since performance depends on the metric, the training dataset, the testing dataset, the computation required, and the downstream task. We systematically investigate the performance of 26 SSL models on eleven datasets to evaluate which metric(s) should be used when benchmarking SSL models.

First, we find that linear and kNN probing accuracies are highly correlated when embedding normalization is applied. They can be used mostly interchangeably and are, on average, the best predictors for OOD metrics. Remarkably, we find that 10%-fine-tuning on ImageNet is the strongest predictor for the ranking of SSL methods in OOD fine-tuning. This is particularly interesting for downstream users who are interested in using SSL pre-trained for transfer learning classification tasks.

Second, we find that linear/kNN probing is more robust to shifts in label granularity and (to some extent) style than fine-tuning protocols. When comparing ID accuracy against OOD accuracy directly, we see that several SSL methods can have equivalent ID fine-tuning results but much weaker OOD fine-tuning results (Fig. 6).

Third, it was previously assumed that discriminative and generative SSL models differ in the type of representations they learn and that generative SSL methods result in powerful, but non-linear representations that require fine-tuning. Using our comprehensive benchmark, we find that differences in performance may be attributed to the differences in the backbone used by different SSL methods.

Fourth, we investigate the importance of embedding normalization on several protocols. We confirm the findings of previous work [65] regarding the impact of batch normalization on batch protocols. In addition, we highlight the effects of batch normalization on end-to-end fine-tuning w.r.t. the dataset size.

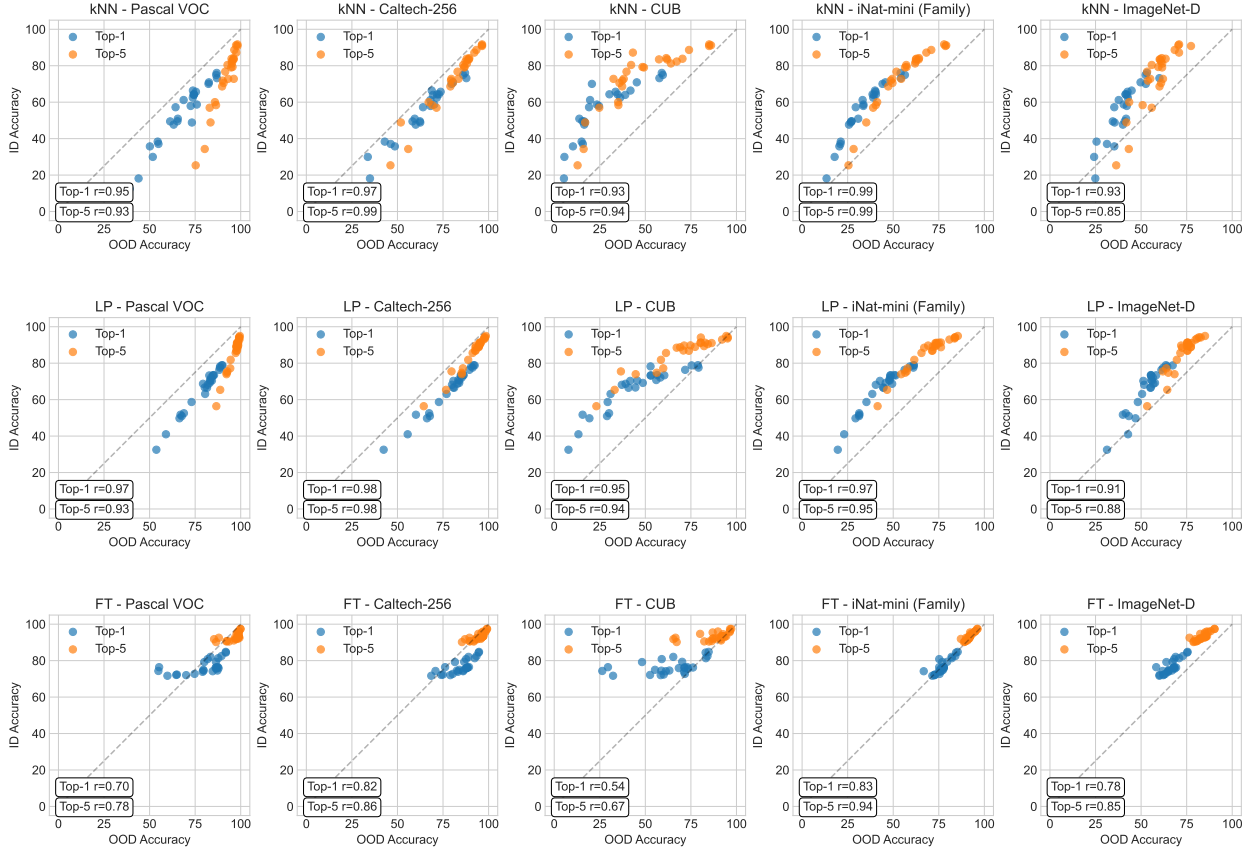


Figure 6: ID vs. OOD accuracy on different protocols and datasets. We compare both top-1 and top-5 classification accuracies. Correlation coefficients r are calculated using Spearman’s rank correlation. ImageNet-D accuracies are averaged across the six datasets. Individual ImageNet-D visualizations can be found in Fig. S.1.

Societal Impact. As the amount of data and applications for AI are growing, self-supervised learning plays an increasingly important role. SSL allows us to train models on unlabeled data and is necessary to reduce human annotation efforts and biases. Therefore, having an SSL evaluation metric that is predictive of various downstream tasks, i.e., of applications in the real world, is critical. In addition, SSL methods are more computationally expensive than supervised learning and, therefore, have a higher environmental impact. We must ensure that evaluation metrics accurately represent the utility of our methods, ensuring that time and resources spent on SSL development are not wasted.

Limitations. Our study has some limitations. While we cover several datasets and evaluation protocols, many more can still be considered. For example, SSL representations are commonly evaluated for other vision tasks like semantic segmentation, object detection, or depth estimation. Evaluating all of these is very costly and, therefore, beyond the scope of this study. Another limitation is categorizing each dataset as ID or OOD in a binary way. In future work, one could try to quantify dataset dissimilarity and use this as a proxy for how far out of distribution a dataset is. Finally, future work should find theoretical grounding for our findings with respect to the interplay between SSL method, backbone, training dataset, and type of domain shift, similar to previous works [73].

Acknowledgments

Manuel Knott was supported by an ETH Zurich Doc.Mobility Fellowship. Pietro Perona and Markus Marks were supported by the National Institutes of Health (NIH R01 MH123612A) and the Caltech Chen Institute (Neuroscience Research Grant Award). Pietro Perona, Neehar Kondapaneni, and Markus Marks were supported by the Simons Foundation (NC-GB-CULM-00002953-02).

References

- [1] F. Locatello, S. Bauer, M. Lucic, G. Raetsch, S. Gelly, B. Schölkopf, and O. Bachem. Challenging Common Assumptions in the Unsupervised Learning of Disentangled Representations. In *Proceedings of the 36th International Conference on Machine Learning (ICML)*, Proceedings of Machine Learning Research, pages 4114–4124. PMLR, 2019. [1](#)
- [2] Kevin Musgrave, Serge Belongie, and Ser-Nam Lim. A Metric Learning Reality Check. In *European Conference on Computer Vision (ECCV)*, pages 681–699, 2020. [1](#)
- [3] Randall Balestrieri, Mark Ibrahim, Vlad Sobal, Ari Morcos, Shashank Shekhar, Tom Goldstein, Florian Bordes, Adrien Bardes, Gregoire Mialon, Yuandong Tian, Avi Schwarzschild, Andrew Gordon Wilson, Jonas Geiping, Quentin Garrido, Pierre Fernandez, Amir Bar, Hamed Pirsiavash, Yann LeCun, and Micah Goldblum. A Cookbook of Self-Supervised Learning. *arXiv preprint arXiv:2304.12210*, 2023. [1](#), [3](#)
- [4] Jennifer J Sun, Markus Marks, Andrew Ulmer, Dipam Chakraborty, Brian Geuther, Edward Hayes, Heng Jia, Vivek Kumar, Sebastian Oleszko, Zachary Partridge, Milan Peelman, Alice Robie, Catherine E Schretter, and others. MABe22: A Multi-Species Multi-Task Benchmark for Learned Representations of Behavior. *International Conference on Machine Learning (ICML)*, 2023. [1](#), [2](#), [3](#)
- [5] Yukun Zhou, Mark A Chia, Siegfried K Wagner, Murat S Ayhan, Dominic J Williamson, Robbert R Struyven, Timing Liu, Moucheng Xu, Mateo G Lozano, Peter Woodward-Court, et al. A foundation model for generalizable disease detection from retinal images. *Nature*, 622(7981):156–163, 2023. [1](#)
- [6] Richard J Chen, Tong Ding, Ming Y Lu, Drew FK Williamson, Guillaume Jaume, Bowen Chen, Andrew Zhang, Daniel Shao, Andrew H Song, Muhammad Shaban, et al. A general-purpose self-supervised model for computational pathology. *arXiv preprint arXiv:2308.15474*, 2023. [1](#)
- [7] Yi Wang, Conrad M Albrecht, Nassim Ait Ali Braham, Lichao Mou, and Xiao Xiang Zhu. Self-supervised learning in remote sensing: A review. *IEEE Geoscience and Remote Sensing Magazine*, 10(4):213–247, 2022. [1](#)
- [8] Yuge Shi, Imant Daunhawer, Julia E. Vogt, Philip Torr, and Amartya Sanyal. How robust are pre-trained models to distribution shift? In *ICML 2022: Workshop on Spurious Correlations, Invariance, and Stability*, 2022. [1](#), [2](#)
- [9] Kaiming He, Xinlei Chen, Saining Xie, Yanghao Li, Piotr Dollár, and Ross B. Girshick. Masked Autoencoders Are Scalable Vision Learners. *2022 IEEE/CVF Conference on Computer Vision and Pattern Recognition (CVPR)*, pages 15979–15988, 2021. [2](#), [3](#), [4](#), [5](#), [8](#), [9](#), [17](#), [18](#), [19](#), [23](#)
- [10] Hangbo Bao, Li Dong, and Furu Wei. BEiT: BERT Pre-Training of Image Transformers. *arXiv preprint arXiv:2106.08254*, 2021. [2](#), [4](#), [5](#), [17](#)
- [11] Xuhong Li, Yves Grandvalet, Franck Davoine, Jingchun Cheng, Yin Cui, Hang Zhang, Serge Belongie, Yi-Hsuan Tsai, and Ming-Hsuan Yang. Transfer learning in computer vision tasks: Remember where you come from. *Image and Vision Computing*, 93:103853, 2020. doi: 10.1016/j.imavis.2019.103853. [2](#)
- [12] Longlong Jing and Yingli Tian. Self-Supervised Visual Feature Learning With Deep Neural Networks: A Survey. *IEEE Transactions on Pattern Analysis and Machine Intelligence*, 43:4037–4058, 2019. [2](#)
- [13] Ting Chen, Simon Kornblith, Kevin Swersky, Mohammad Norouzi, and Geoffrey E Hinton. Big self-supervised models are strong semi-supervised learners. *Advances in neural information processing systems*, 33:22243–22255, 2020. [2](#)
- [14] Ting Chen, Simon Kornblith, Mohammad Norouzi, and Geoffrey Hinton. A Simple Framework for Contrastive Learning of Visual Representations. In *Proceedings of the 37th International Conference on Machine Learning*, volume 119 of *Proceedings of Machine Learning Research*, pages 1597–1607. PMLR, 2020. [2](#), [3](#), [4](#), [17](#), [18](#), [19](#)

[15] Ishan Misra and Laurens van der Maaten. Self-Supervised Learning of Pretext-Invariant Representations. *2020 IEEE/CVF Conference on Computer Vision and Pattern Recognition (CVPR)*, pages 6706–6716, 2019. [2](#), [4](#), [17](#), [18](#), [19](#)

[16] Jean-Bastien Grill, Florian Strub, Florent Altché, Corentin Tallec, Pierre H. Richemond, Elena Buchatskaya, Carl Doersch, Bernardo Avila Pires, Zhaoan Daniel Guo, Mohammad Gheshlaghi Azar, Bilal Piot, Koray Kavukcuoglu, Rémi Munos, and Michal Valko. Bootstrap Your Own Latent a New Approach to Self-Supervised Learning. In *Proceedings of the 34th International Conference on Neural Information Processing Systems*, 2020. [2](#), [3](#), [4](#), [17](#), [18](#), [19](#), [23](#)

[17] Jinghao Zhou, Chen Wei, Huiyu Wang, Wei Shen, Cihang Xie, Alan Yuille, and Tao Kong. iBOT: Image BERT Pre-Training with Online Tokenizer. *arXiv preprint arXiv:2111.07832*, 2021. [2](#), [3](#), [4](#), [9](#), [17](#), [18](#), [19](#)

[18] Chethan Pandarinath, Daniel J O’Shea, Jasmine Collins, Rafal Jozefowicz, Sergey D Stavisky, Jonathan C Kao, Eric M Trautmann, Matthew T Kaufman, Stephen I Ryu, Leigh R Hochberg, Henderson, Jaimie M, Shenoy, Krishna V, Abbott, L F, and Sussillo, David. Inferring single-trial neural population dynamics using sequential auto-encoders. *Nature methods*, 15(10):805–815, 2018. [2](#)

[19] Irina Higgins, Le Chang, Victoria Langston, Demis Hassabis, Christopher Summerfield, Doris Tsao, and Matthew Botvinick. Unsupervised deep learning identifies semantic disentanglement in single inferotemporal face patch neurons. *Nature communications*, 12(1):6456, 2021. [2](#)

[20] Xipeng Qiu, Tianxiang Sun, Yige Xu, Yunfan Shao, Ning Dai, and Xuanjing Huang. Pre-trained models for natural language processing: A survey. *Science China Technological Sciences*, 63(10):1872–1897, 2020. [3](#)

[21] Jacob Devlin, Ming-Wei Chang, Kenton Lee, and Kristina Toutanova. BERT: Pre-training of Deep Bidirectional Transformers for Language Understanding. In *Proceedings of the 2019 Conference of the North American Chapter of the Association for Computational Linguistics: Human Language Technologies*, pages 4171–4186, 2019. [3](#)

[22] Mathilde Caron, Hugo Touvron, Ishan Misra, Hervé Jégou, Julien Mairal, Piotr Bojanowski, and Armand Joulin. Emerging Properties in Self-Supervised Vision Transformers. In *Proceedings of the IEEE/CVF International Conference on Computer Vision (ICCV)*, pages 9650–9660, 2021. [3](#), [4](#), [17](#), [18](#), [19](#), [23](#)

[23] Aäron van den Oord, Yazhe Li, and Oriol Vinyals. Representation learning with contrastive predictive coding. *arXiv preprint arXiv:1807.03748*, 2018. [3](#)

[24] Christoph Feichtenhofer, Haoqi Fan, Yanghao Li, and Kaiming He. Masked autoencoders as spatiotemporal learners. *Advances in neural information processing systems*, 32:35946–35958, 2022. [3](#), [5](#), [8](#)

[25] Xumin Yu, Lulu Tang, Yongming Rao, Tiejun Huang, Jie Zhou, and Jiwen Lu. Point-bert: Pre-training 3d point cloud transformers with masked point modeling. In *Proceedings of the IEEE/CVF Conference on Computer Vision and Pattern Recognition*, pages 19313–19322, 2022. [3](#)

[26] Xiao Liu, Fanjin Zhang, Zhenyu Hou, Li Mian, Zhaoyu Wang, Jing Zhang, and Jie Tang. Self-supervised learning: Generative or contrastive. *IEEE Transactions on Knowledge and Data Engineering*, 33(1): 857–876, 2021. [3](#), [5](#)

[27] Kaiming He, Haoqi Fan, Yuxin Wu, Saining Xie, and Ross B. Girshick. Momentum Contrast for Unsupervised Visual Representation Learning. *2020 IEEE/CVF Conference on Computer Vision and Pattern Recognition (CVPR)*, pages 9726–9735, 2019. [3](#)

[28] Mathilde Caron, Ishan Misra, Julien Mairal, Priya Goyal, Piotr Bojanowski, and Armand Joulin. Unsupervised Learning of Visual Features by Contrasting Cluster Assignments. *Advances in Neural Information Processing Systems*, 33:9912–9924, 2020. [3](#), [4](#), [17](#), [18](#), [19](#), [23](#)

[29] Mathilde Caron, Piotr Bojanowski, Armand Joulin, and Matthijs Douze. Deep Clustering for Unsupervised Learning of Visual Features. In *European Conference on Computer Vision (ECCV)*, 2018. [3](#), [18](#), [19](#)

[30] Xueting Yan, Ishan Misra, Abhinav Kumar Gupta, Deepti Ghadiyaram, and Dhruv Kumar Mahajan. ClusterFit: Improving Generalization of Visual Representations. *2020 IEEE/CVF Conference on Computer Vision and Pattern Recognition (CVPR)*, pages 6508–6517, 2019. [3](#), [18](#), [19](#)

[31] Ashish Vaswani, Noam Shazeer, Niki Parmar, Jakob Uszkoreit, Llion Jones, Aidan N. Gomez, Łukasz Kaiser, and Illia Polosukhin. Attention is All you Need. In *Advances in Neural Information Processing Systems (NeurIPS)*, pages 6000–6010, 2017. [3](#)

[32] Chen Wei, Haoqi Fan, Saining Xie, Chao-Yuan Wu, Alan Yuille, and Christoph Feichtenhofer. Masked Feature Prediction for Self-Supervised Visual Pre-Training. In *2022 IEEE/CVF Conference on Computer Vision and Pattern Recognition (CVPR)*, pages 14648–14658, 2022. doi: 10.1109/CVPR52688.2022.01426. [3](#), [4](#), [5](#), [8](#), [9](#), [17](#), [18](#), [19](#)

[33] N. Dalal and B. Triggs. Histograms of Oriented Gradients for Human Detection. In *2005 IEEE Computer Society Conference on Computer Vision and Pattern Recognition*, volume 1, pages 886–893, 2005. [3](#)

[34] Yuxin Fang, Wen Wang, Binhui Xie, Quan-Sen Sun, Ledell Yu Wu, Xinggang Wang, Tiejun Huang, Xinlong Wang, and Yue Cao. EVA: Exploring the Limits of Masked Visual Representation Learning at Scale. *2023 IEEE/CVF Conference on Computer Vision and Pattern Recognition (CVPR)*, pages 19358–19369, 2022. [3](#), [18](#), [19](#)

[35] Zejiang Hou, Fei Sun, Yen-Kuang Chen, Yuan Xie, and Sun-Yuan Kung. MILAN: Masked image pretraining on language assisted representation. *arXiv preprint arXiv:2208.06049*, 2022. [3](#), [4](#), [17](#), [18](#), [19](#)

[36] Yuan Liu, Songyang Zhang, Jiacheng Chen, Kai Chen, and Dahua Lin. Pixmim: Rethinking pixel reconstruction in masked image modeling. *arXiv preprint arXiv:2303.02416*, 2023. [3](#), [17](#), [18](#), [19](#)

[37] Zhirong Wu, Yuanjun Xiong, Stella X. Yu, and Dahua Lin. Unsupervised Feature Learning via Non-parametric Instance Discrimination. *2018 IEEE/CVF Conference on Computer Vision and Pattern Recognition*, pages 3733–3742, 2018. [4](#), [17](#), [18](#), [19](#)

[38] Ira Assent. Clustering high dimensional data. *Wiley Interdisciplinary Reviews: Data Mining and Knowledge Discovery*, 2(4):340–350, 2012. [4](#)

[39] Xinlei Chen, Haoqi Fan, Ross Girshick, and Kaiming He. Improved Baselines with Momentum Contrastive Learning. *arXiv preprint arXiv:2003.04297*, 2020. [4](#), [17](#), [18](#), [19](#)

[40] Mark Chen, Alec Radford, Rewon Child, Jeffrey Wu, Heewoo Jun, David Luan, and Ilya Sutskever. Generative Pretraining From Pixels. In *Proceedings of the 37th International Conference on Machine Learning*, volume 119, pages 1691–1703. PMLR, 2020. [4](#), [17](#)

[41] Xiaoyi Dong, Jianmin Bao, Ting Zhang, Dongdong Chen, Weiming Zhang, Lu Yuan, Dong Chen, Fang Wen, Nenghai Yu, and Baining Guo. PeCo: Perceptual Codebook for BERT Pre-training of Vision Transformers. In *Proceedings of the AAAI Conference on Artificial Intelligence*, volume 37, pages 552–560, 2023. [4](#), [17](#)

[42] Zhenda Xie, Zheng Zhang, Yue Cao, Yutong Lin, Jianmin Bao, Zhuliang Yao, Qi Dai, and Han Hu. SimMIM: A Simple Framework for Masked Image Modeling. *2022 IEEE/CVF Conference on Computer Vision and Pattern Recognition (CVPR)*, 2021. [17](#)

[43] Priya Goyal, Mathilde Caron, Benjamin Lefauveux, Min Xu, Pengchao Wang, Vivek Pai, Mannat Singh, Vitaliy Liptchinsky, Ishan Misra, Armand Joulin, and Piotr Bojanowski. Self-supervised Pretraining of Visual Features in the Wild. *arXiv preprint arXiv:2103.01988*, 2021. [4](#), [17](#)

[44] Carl Doersch, Abhinav Gupta, and Alexei A. Efros. Unsupervised Visual Representation Learning by Context Prediction. *2015 IEEE International Conference on Computer Vision (ICCV)*, pages 1422–1430, 2015. [4](#)

[45] Deepak Pathak, Philipp Krähenbühl, Jeff Donahue, Trevor Darrell, and Alexei A. Efros. Context Encoders: Feature Learning by Inpainting. *2016 IEEE Conference on Computer Vision and Pattern Recognition (CVPR)*, pages 2536–2544, 2016.

[46] Richard Zhang, Phillip Isola, and Alexei A. Efros. Split-Brain Autoencoders: Unsupervised Learning by Cross-Channel Prediction. *2017 IEEE Conference on Computer Vision and Pattern Recognition (CVPR)*, pages 645–654, 2016. [4](#)

[47] Xinlei Chen, Saining Xie, and Kaiming He. An Empirical Study of Training Self-Supervised Vision Transformers. In *2021 IEEE/CVF International Conference on Computer Vision (ICCV)*, pages 9620–9629, 2021. [4](#), [17](#), [18](#), [19](#)

[48] Mehdi Noroozi and Paolo Favaro. Unsupervised Learning of Visual Representations by Solving Jigsaw Puzzles. In *European Conference on Computer Vision (ECCV)*, 2016. [4](#), [17](#), [18](#), [19](#)

[49] Jason Yosinski, Jeff Clune, Yoshua Bengio, and Hod Lipson. How transferable are features in deep neural networks? In *Advances in Neural Information Processing Systems*, volume 27, 2014. [4](#)

[50] Wouter Van Gansbeke, Simon Vandenhende, Stamatis Georgoulis, Marc Proesmans, and Luc Van Gool. SCAN: Learning to Classify Images Without Labels. In *European Conference on Computer Vision*, 2020. [4](#)

[51] Donghyun Kim, Kaihong Wang, Stan Sclaroff, and Kate Saenko. A broad study of pre-training for domain generalization and adaptation. In *European Conference on Computer Vision*, pages 621–638. Springer, 2022. 4

[52] Linyi Yang, Shuibai Zhang, Libo Qin, Yafu Li, Yidong Wang, Hanmeng Liu, Jindong Wang, Xing Xie, and Yue Zhang. GLUE-X: Evaluating Natural Language Understanding Models from an Out-of-distribution Generalization Perspective. *arXiv preprint arXiv:2211.08073*, 2022. 4

[53] Ananya Kumar, Aditi Raghunathan, Robbie Jones, Tengyu Ma, and Percy Liang. Fine-Tuning can Distort Pretrained Features and Underperform Out-of-Distribution. *arXiv preprint arXiv:2202.10054*, 2022. 5

[54] Alejandro Newell and Jia Deng. How Useful Is Self-Supervised Pretraining for Visual Tasks? In *Proceedings of the IEEE/CVF Conference on Computer Vision and Pattern Recognition (CVPR)*, June 2020. 5

[55] Jeff Z HaoChen, Colin Wei, Ananya Kumar, and Tengyu Ma. Beyond separability: Analyzing the linear transferability of contrastive representations to related subpopulations. *arXiv preprint arXiv:2204.02683*, 2022. 5

[56] Mark Ibrahim, Quentin Garrido, Ari Morcos, and Diane Bouchacourt. The robustness limits of sota vision models to natural variation. *arXiv preprint arXiv:2210.13604*, 2022. 5

[57] Linus Ericsson, Henry Gouk, and Timothy M Hospedales. How well do self-supervised models transfer? In *Proceedings of the IEEE/CVF Conference on Computer Vision and Pattern Recognition*, pages 5414–5423, 2021. 5

[58] Matthew Gwilliam and Abhinav Shrivastava. Beyond supervised vs. unsupervised: Representative benchmarking and analysis of image representation learning. In *Proceedings of the IEEE/CVF Conference on Computer Vision and Pattern Recognition*, pages 9642–9652, 2022. 5

[59] John P Miller, Rohan Taori, Aditi Raghunathan, Shiori Sagawa, Pang Wei Koh, Vaishaal Shankar, Percy Liang, Yair Carmon, and Ludwig Schmidt. Accuracy on the line: on the strong correlation between out-of-distribution and in-distribution generalization. In *International Conference on Machine Learning*, pages 7721–7735. PMLR, 2021. 5

[60] Alex Krizhevsky and Geoffrey Hinton. Learning multiple layers of features from tiny images, 2009. URL <https://www.cs.utoronto.ca/~kriz/learning-features-2009-TR.pdf>. 5

[61] Benjamin Recht, Rebecca Roelofs, Ludwig Schmidt, and Vaishaal Shankar. Do imagenet classifiers generalize to imagenet? In *International conference on machine learning*, pages 5389–5400. PMLR, 2019. 5

[62] Elijah Cole, Xuan Yang, Kimberly Wilber, Oisin Mac Aodha, and Serge Belongie. When does contrastive visual representation learning work? In *Proceedings of the IEEE/CVF Conference on Computer Vision and Pattern Recognition (CVPR)*, pages 14755–14764, 2022. 5, 6, 21

[63] Micah Goldblum, Hossein Souri, Renkun Ni, Manli Shu, Viraj Prabhu, Gowthami Somepalli, Prithvijit Chattopadhyay, Mark Ibrahim, Adrien Bardes, Judy Hoffman, and others. Battle of the backbones: A large-scale comparison of pretrained models across computer vision tasks. *Advances in Neural Information Processing Systems*, 36, 2024. 5

[64] Jiahui Yu, Xin Li, Jing Yu Koh, Han Zhang, Ruoming Pang, James Qin, Alexander Ku, Yuanzhong Xu, Jason Baldridge, and Yonghui Wu. Vector-quantized image modeling with improved VQGAN. *arXiv preprint arXiv:2110.04627*, 2021. 5

[65] Jae-Hun Lee, Doyoung Yoon, ByeongMoon Ji, Kyungyul Kim, and Sangheum Hwang. Rethinking evaluation protocols of visual representations learned via self-supervised learning. *arXiv preprint arXiv:2304.03456*, 2023. 5, 8, 10, 23

[66] Olga Russakovsky, Jia Deng, Hao Su, Jonathan Krause, Sanjeev Satheesh, Sean Ma, Zhiheng Huang, Andrej Karpathy, Aditya Khosla, Michael Bernstein, Alexander C. Berg, and Li Fei-Fei. ImageNet Large Scale Visual Recognition Challenge. *International Journal of Computer Vision*, 115(3):211–252, December 2015. doi: 10.1007/s11263-015-0816-y. 5

[67] Gregory Griffin, Alex Holub, and Pietro Perona. Caltech 256, 2022. URL <https://data.caltech.edu/records/20087>. 6

[68] Mark Everingham, Luc Van Gool, Christopher K. I. Williams, John Winn, and Andrew Zisserman. The Pascal Visual Object Classes (VOC) Challenge. *International Journal of Computer Vision*, 88(2):303–338, 2010. doi: 10.1007/s11263-009-0275-4. 6

[69] Grant Van Horn, Elijah Cole, Sara Beery, Kimberly Wilber, Serge Belongie, and Oisin Mac Aodha. Benchmarking representation learning for natural world image collections. In *Proceedings of the IEEE/CVF conference on computer vision and pattern recognition*, pages 12884–12893, 2021. [6](#)

[70] Catherine Wah, Steve Branson, Peter Welinder, Pietro Perona, and Serge Belongie. The Caltech-UCSD Birds-200-2011 Dataset, 2011. CNS-TR-2011-001. [6](#)

[71] Evgenia Rusak, Steffen Schneider, Peter Vincent Gehler, Oliver Bringmann, Wieland Brendel, and Matthias Bethge. ImageNet-D: A new challenging robustness dataset inspired by domain adaptation. In *ICML 2022 Shift Happens Workshop*, 2022. [6](#)

[72] Zhiliang Peng, Li Dong, Hangbo Bao, Qixiang Ye, and Furu Wei. BEiT v2: Masked Image Modeling with Vector-Quantized Visual Tokenizers. *arXiv preprint arXiv:2208.06366*, 2022. [8](#), [18](#), [19](#)

[73] Vivien Cabannes, Bobak Kiani, Randall Balestrieri, Yann LeCun, and Alberto Bietti. The ssl interplay: Augmentations, inductive bias, and generalization. In *International Conference on Machine Learning*, pages 3252–3298. PMLR, 2023. [11](#)

[74] Xinlei Chen and Kaiming He. Exploring Simple Siamese Representation Learning. *2021 IEEE/CVF Conference on Computer Vision and Pattern Recognition (CVPR)*, pages 15745–15753, 2020. [17](#), [18](#), [19](#)

[75] Jure Zbontar, Li Jing, Ishan Misra, Yann LeCun, and Stéphane Deny. Barlow Twins: Self-Supervised Learning via Redundancy Reduction. In *International Conference on Machine Learning*, 2021. [17](#), [18](#), [19](#), [23](#)

[76] Alexei Baevski, Wei-Ning Hsu, Qiantong Xu, Arun Babu, Jiatao Gu, and Michael Auli. data2vec: A General Framework for Self-supervised Learning in Speech, Vision and Language. In *International Conference on Machine Learning (ICML)*, 2022. [17](#)

[77] Xiaokang Chen, Mingyu Ding, Xiaodi Wang, Ying Xin, Shentong Mo, Yunhao Wang, Shumin Han, Ping Luo, Gang Zeng, and Jingdong Wang. Context Autoencoder for Self-Supervised Representation Learning. *International Journal of Computer Vision*, 132(1):208–223, 2024. [17](#)

[78] Spyros Gidaris, Praveer Singh, and Nikos Komodakis. Unsupervised Representation Learning by Predicting Image Rotations. In *International Conference on Learning Representations*, 2018. [18](#), [19](#)

[79] Yuki Markus Asano, Christian Rupprecht, and Andrea Vedaldi. Self-labelling via simultaneous clustering and representation learning. In *International Conference on Learning Representations*, 2020. [18](#), [19](#)

[80] Xinlong Wang, Rufeng Zhang, Chunhua Shen, Tao Kong, and Lei Li. Dense Contrastive Learning for Self-Supervised Visual Pre-Training. *2021 IEEE/CVF Conference on Computer Vision and Pattern Recognition (CVPR)*, pages 3023–3032, 2020. [18](#), [19](#)

[81] Adam Paszke, Sam Gross, Francisco Massa, Adam Lerer, James Bradbury, Gregory Chanan, Trevor Killeen, Zeming Lin, Natalia Gimelshein, Luca Antiga, Alban Desmaison, Andreas Kopf, Edward Yang, Zachary DeVito, Martin Raison, Alykhan Tejani, Sasank Chilamkurthy, Benoit Steiner, Lu Fang, Junjie Bai, and Soumith Chintala. PyTorch: An Imperative Style, High-Performance Deep Learning Library. *Advances in Neural Information Processing Systems (NeurIPS)*, 32:8026–8037, 2019. [23](#)

[82] Ross Wightman. PyTorch Image Models, 2019. URL <https://github.com/rwightman/pytorch-image-models>. [23](#)

[83] MMSelfSup Contributors. MMSelfSup: OpenMMLab Self-Supervised Learning Toolbox and Benchmark, 2021. URL <https://github.com/open-mmlab/mmselfsup>. [23](#)

[84] Fabian Pedregosa, Gaël Varoquaux, Alexandre Gramfort, Vincent Michel, Bertrand Thirion, Olivier Grisel, Mathieu Blondel, Peter Prettenhofer, Ron Weiss, and Vincent Dubourg. Scikit-learn: Machine learning in Python. *Journal of Machine Learning Research*, 12:2825–2830, 2011. [23](#)

[85] Alexander Kolesnikov, Xiaohua Zhai, and Lucas Beyer. Revisiting Self-Supervised Visual Representation Learning. *2019 IEEE/CVF Conference on Computer Vision and Pattern Recognition (CVPR)*, pages 1920–1929, 2019. [23](#)

Supplementary Materials

A Protocol Survey

Tab. S.1 shows the survey on classification-based SSL evaluation protocols we conducted at the beginning of this study. We decided to include the most protocols and to exclude very rarely used ones, i.e., partial fine-tuning and probing with a Support Vector Machine. Note that many papers additionally evaluate task transfer learning (e.g., semantic segmentation, object detection, image retrieval, or video classification), which is not covered in this survey.

Table S.1: Survey on classification-based evaluation protocols for self-supervised learning in a selection of papers. A ✓ denotes that the protocol was used in the mentioned paper. knn: k-nearest neighbors probing, LP: linear probing, FT: fine-tuning, FSFT: few-shot fine-tuning (1% or 10%), PFT: partial fine-tuning, SVM: SVM probing, CM: clustering metrics. Note that many papers additionally evaluate task transfer learning (typically on object detection or semantic segmentation tasks) which is not covered in this table.

Method	Year	In domain					Out of domain			
		knn	LP	FT	FSFT	PFT	SVM	knn	LP	FT
Jigsaw [48]	2016			✓						✓
npid [37]	2018	✓		✓	✓			✓		
PIRL [15]	2019		✓	✓	✓				✓	✓
BYOL [16]	2020		✓		✓				✓	✓
SimCLR [14]	2020		✓	✓	✓				✓	✓
MoCo v2 [39]	2020		✓						✓	✓
ImageGPT [40]	2020			✓	✓				✓	✓
SwAV [28]	2020	✓		✓	✓			✓		✓
SimSiam [74]	2020	✓	✓							
DINO [22]	2021	✓	✓	✓	✓	✓			✓	
MAE [9]	2021		✓	✓			✓			✓
BEiT [10]	2021		✓	✓						✓
MoCo v3 [47]	2021	✓	✓	✓						
SimMIM [42]	2021		✓	✓						
iBOT [17]	2021	✓	✓	✓	✓					✓
MaskFeat [32]	2021				✓					
SEER [43]	2021		✓	✓	✓				✓	✓
Barlow Twins [75]	2021		✓			✓			✓	
data2vec [76]	2022				✓					
MILAN [35]	2022		✓	✓						
PeCo [41]	2023		✓	✓						
PixMIM [36]	2023		✓	✓	✓					
CAE [77]	2024		✓	✓						✓

B Full Result Tables

(next page)

Table S.2: *Top-1* classification accuracies (in %). LP: Linear Probing, FT: End-to-end Fine-tuning, FT 10%/1%: Few-Shot Fine-tuning on 10%/1% of the training data, kNN: k-nearest neighbors probing. The superscript “BN” denotes the use of a final batch norm layer. The superscript “N” is the equivalent for k-nearest neighbors probing where the embedding is normalization on training split statistics.

Method	Backbone	Imagenet						PascalVOC						Cifar100						Caltech-256						CUB					
		kNN	kNN ^N	LP	LP ^{BN}	FT	FT10%	FT10% ^{BN}	FT1%	FT1% ^{BN}	kNN	kNN ^N	LP	LP ^{BN}	FT	kNN	kNN ^N	LP	LP ^{BN}	FT	kNN	kNN ^N	LP	LP ^{BN}	FT	kNN	kNN ^N	LP	LP ^{BN}	FT	
Jigsaw [48]	RN-50	12.0	12.4	28.6	32.5	72.2	50.9	53.8	17.0	22.2	39.0	39.1	44.7	53.7	64.6	26.7	27.6	34.7	66.7	77.5	26.7	27.3	29.4	42.4	74.0	3.4	4.1	5.1	7.8	52.6	
rotnet [78]	RN-50	18.5	18.1	35.3	41.0	72.4	52.7	55.2	20.1	24.4	42.0	44.0	52.3	59.0	65.6	38.5	38.4	37.5	46.9	79.6	34.5	34.9	41.5	55.6	74.9	5.2	5.3	7.6	13.3	60.1	
upid [37]	RN-50	36.7	37.1	31.5	51.0	71.7	50.5	56.2	10.2	29.9	55.4	54.9	32.5	67.7	59.8	40.4	39.9	23.3	56.5	78.6	46.5	46.3	16.3	67.8	68.5	15.8	15.7	10.7	29.0	32.3	
Sela-v2 [79]	RN-50	60.4	61.2	70.4	70.3	75.9	68.4	68.6	50.5	55.5	73.3	68.7	82.1	83.4	87.9	59.2	57.6	37.9	46.5	85.4	68.6	68.0	74.2	80.7	87.7	17.3	19.7	21.1	41.7	68.4	
upid++ [15, 37]	RN-50	36.8	38.4	54.0	52.5	72.7	56.7	58.7	27.4	32.8	55.4	54.5	70.5	68.8	74.7	39.0	38.5	43.6	54.6	82.4	43.3	43.0	63.9	69.4	14.4	15.0	22.2	30.1	71.7		
PIRL [15]	RN-50	49.0	49.5	58.1	58.7	73.8	59.9	60.9	33.4	39.5	64.5	61.3	75.1	73.0	79.1	47.7	45.3	35.8	49.2	83.4	57.4	58.2	69.9	72.7	83.2	16.2	16.4	21.5	29.3	71.3	
clusterfit [30]	RN-50	35.0	35.7	48.6	49.8	72.0	54.3	56.2	25.2	30.3	54.0	50.2	66.2	66.4	70.1	49.4	48.9	62.0	62.2	81.0	42.6	48.6	66.6	66.2	79.0	7.2	10.3	18.0	19.3	58.4	
Deepcluster-v2 [28, 29]	RN-50	64.8	65.7	74.7	73.5	76.5	69.6	70.0	50.0	57.4	75.1	75.4	85.7	85.4	87.9	63.1	63.0	45.6	48.6	85.9	73.3	73.7	83.4	86.1	89.2	27.1	33.7	39.1	56.5	73.0	
SwAV [28]	RN-50	63.2	64.3	74.1	73.2	76.3	69.0	70.3	46.0	56.7	73.9	74.2	84.3	84.9	86.5	62.2	62.7	43.8	47.4	85.5	72.4	72.7	80.7	84.7	88.3	24.1	30.3	30.9	52.9	71.4	
SimCLR [14]	RN-50	58.1	57.2	66.9	68.1	74.6	65.8	66.6	47.6	53.6	73.1	64.2	81.4	81.9	87.2	55.6	51.9	33.5	50.9	85.1	64.5	64.0	70.4	79.9	86.1	18.4	19.1	18.8	37.1	63.2	
MoCo v2 [39]	RN-50	59.4	58.7	60.0	70.4	75.0	61.6	63.9	27.2	48.9	78.3	75.9	80.7	84.2	87.9	58.7	57.3	29.3	66.5	83.9	70.4	70.2	39.0	84.0	83.9	20.4	23.4	13.0	45.6	55.3	
SimSiam [74]	RN-50	57.5	57.9	38.1	69.2	74.3	53.7	61.7	8.5	40.2	76.0	72.5	16.0	83.0	54.8	61.4	58.3	20.4	61.2	79.3	69.7	68.1	7.8	83.9	70.9	22.4	24.6	9.6	48.6	26.4	
BYOL [16]	RN-50	63.2	64.0	72.7	72.1	75.6	68.2	68.0	50.0	56.3	75.6	74.3	84.3	83.8	86.6	62.7	59.4	54.2	60.5	85.8	71.0	69.5	81.8	85.3	87.5	35.3	39.0	40.2	58.2	73.4	
Barlow Twins [75]	RN-50	61.8	62.5	71.5	70.8	74.2	66.2	65.2	47.4	51.4	76.1	73.7	83.8	82.2	84.6	61.6	58.4	51.7	57.7	84.1	73.0	71.6	81.9	83.4	86.0	30.4	36.2	42.2	56.0	61.2	
DenseCL [80]	RN-50	48.2	48.8	49.3	63.1	74.5	59.3	61.9	26.8	42.7	75.6	73.2	80.5	79.7	84.7	49.8	47.4	27.1	56.5	83.7	62.0	62.5	49.6	77.0	82.6	14.9	16.9	10.4	30.9	58.8	
DINO [22]	RN-50	64.1	64.2	74.4	73.3	76.0	68.4	69.5	49.2	55.5	75.7	74.4	83.5	82.8	86.2	58.8	56.5	46.0	49.5	85.3	73.1	71.7	81.1	85.0	88.3	31.3	34.8	32.0	53.0	71.6	
MoCo v3 [47]	RN-50	66.2	66.4	74.5	73.4	76.2	69.4	70.3	51.3	59.1	76.7	73.8	86.1	84.8	87.2	64.4	59.2	58.0	61.5	86.2	73.6	68.8	85.2	86.3	88.5	43.4	41.9	49.0	60.4	76.2	
DINO [22]	ViT-B/16	74.7	74.9	76.7	77.6	81.3	75.4	76.6	65.9	69.2	86.5	86.5	87.6	88.6	87.7	76.5	77.0	32.0	86.0	90.6	85.7	86.0	90.4	91.2	92.4	58.4	59.6	78.2	79.2	83.2	
iBOT [17]	ViT-B/16	75.8	76.0	78.2	78.9	82.5	77.7	78.7	68.8	71.8	87.0	86.8	88.1	89.7	89.5	76.7	76.9	82.8	83.2	92.2	86.5	87.0	91.3	91.8	93.4	57.4	59.0	78.2	78.4	84.1	
MoCo v3 [47]	ViT-B/16	70.3	70.9	73.9	76.3	80.8	74.4	74.8	34.6	66.0	81.8	82.5	80.9	88.3	81.9	75.2	75.9	8.6	76.3	83.3	79.0	80.5	89.5	87.7	87.4	43.4	45.3	39.4	71.8	59.0	
MAE [9]	ViT-B/16	26.6	47.7	58.7	66.7	79.3	68.0	69.7	49.7	54.2	34.5	36.2	50.5	50.3	86.4	22.3	48.7	42.2	66.7	85.3	28.7	60.0	34.6	86.6	5.5	16.5	7.1	44.5	70.2		
MaskFeat [32]	ViT-B/16	13.7	30.0	3.7	51.7	76.4	56.5	64.8	7.7	43.7	34.6	51.8	16.0	67.0	55.2	29.8	44.2	44.6	9.6	58.7	84.2	21.3	33.7	6.4	60.1	76.1	4.0	5.6	1.5	25.6	29.5
BEiT v2 [72]	ViT-B/16	69.1	70.0	78.4	78.2	84.8	80.5	80.7	68.2	72.8	82.1	82.3	88.1	88.7	91.8	74.0	74.4	8.0	83.0	83.0	92.3	79.0	79.7	90.2	90.5	94.7	19.5	20.7	50.7	52.9	84.7
MILAN [35]	ViT-B/16	72.9	73.2	76.4	78.8	84.4	78.9	79.0	67.3	69.4	87.3	87.0	90.9	90.0	91.9	70.6	71.2	70.9	79.7	90.0	87.7	88.2	92.4	94.5	95.6	57.7	52.0	75.4	83.1	83.3	
EVA [34]	ViT-B/16	47.1	50.9	60.5	68.7	82.1	71.6	72.9	41.1	52.5	61.0	65.5	67.5	73.0	84.3	55.2	50.1	54.6	76.6	87.4	53.9	59.5	29.8	82.8	89.0	11.6	13.8	9.0	39.1	65.3	
PixMIM [36]	ViT-B/16	39.4	49.5	59.3	66.5	79.2	63.3	66.1	25.9	44.3	51.9	65.3	50.4	81.5	80.0	43.4	57.5	50.0	71.8	81.1	47.6	62.3	35.8	81.1	81.5	9.6	15.5	8.0	40.8	48.2	

Method	Backbone	Imagenet-D						Cifar100						Caltech-256						CUB												
		Clipart	Infograph	Painting	Quickdraw	Real	Sketch	kNN	kNN ^N	LP	LP ^{BN}	FT	kNN	kNN ^N	LP	LP ^{BN}	FT	kNN	kNN ^N	LP	LP ^{BN}	FT	kNN	kNN ^N	LP	LP ^{BN}	FT					
Jigsaw [48]	RN-50	16.0	16.7	22.1	35.7	65.0	8.8	8.7	9.8	13.4	31.3	15.0	15.1	23.1	32.1	57.5	30.9	32.5	16.4	26.5	71.7	29.2	29.4	43.0	53.0	76.2	14.5	15.1	17.7	27.1	59.1	
rotnet [78]	RN-50	23.7	24.7	34.5	46.9	68.2	9.0	10.0	12.9	17.8	34.6	21.7	21.7	34.0	41.9	60.8	35.4	35.0	49.7	49.7	72.0	36.3	36.5	52.2	60.3	77.4	20.5	21.4	29.3	40.4	62.2	
upid [37]	RN-50	29.1	28.4	10.6	47.3	65.3	14.0	14.2	5.3	19.1	31.4	30.7	31.0	16.8	45.2	57.4	40.6	37.4	8.4	45.1	70.7	50.5	50.8	36.6	64.3	76.1	25.9	25.8	9.6	38.5	59.3	
Sela-v2 [79]	RN-50	35.4	34.3	48.8	55.2	74.1	17.8	18.9	22.5	25.7	42.4	45.3	45.9	56.6	59.1	70.2	32.1	27.2	33.2	42.8	42.8	70.6	65.9	67.5	75.3	75.9	82.3	32.1	32.4	44.0	48.7	67.7
upid++ [15, 37]	RN-50	23.5	22.1	40.5	45.6	69.3	13.8	13.8	17.2	20.4	35.6	35.0	29.2	29.2	29.2	43.6	45.2	29.4	17.9	24.7	24.6	32.2	39.8	37.5	32.0	31.2	40.9	46.7	64.6			
PIRL [15]	RN-50	34.9	34.0	47.8	54.4	71.4	16.4	17.7	20.1	23.8	37.9	39.8	50.1	52.6	64.7	33.0	34.5	23.6	46.4	73.7	24.1	24.2	39.7	4								

Table S.3: *Top-5* classification accuracies (in %). LP: Linear Probing, FT: End-to-end Fine-tuning, FT 10%/1%: Few-Shot Fine-tuning on 10%/1% of the training data, kNN: k-nearest neighbors probing. The superscript “BN” denotes the use of a final batch norm layer. The superscript “N” is the equivalent for k-nearest neighbors probing where the embedding is normalization on training split statistics.

Method	Backbone	Imagenet						PascalVOC						Cifar100						Caltech-256						CUB					
		kNN	kNN ^N	LP	LP ^{BN}	FT	FT10%	FT10% ^{BN}	FT1%	FT1% ^{BN}	kNN	kNN ^N	LP	LP ^{BN}	FT	kNN	kNN ^N	LP	LP ^{BN}	FT	kNN	kNN ^N	LP	LP ^{BN}	FT	kNN	kNN ^N	LP	LP ^{BN}	FT	
Jigsaw [48]	RN-50	24.8	25.4	52.2	56.4	90.5	76.6	77.9	39.3	45.8	75.6	75.3	85.1	86.6	92.1	51.8	52.7	54.2	65.6	94.8	45.3	46.2	50.4	64.4	89.7	11.4	12.8	16.4	23.1	82.3	
rotnet [78]	RN-50	34.8	34.3	59.8	65.4	90.7	78.0	78.8	42.8	48.3	79.4	80.3	87.9	88.8	92.4	66.7	66.1	65.7	74.3	95.4	55.8	55.9	66.0	76.7	89.6	16.1	16.1	23.5	33.1	86.5	
upid [37]	RN-50	57.9	58.4	56.5	74.8	90.2	76.5	79.7	27.1	54.8	87.0	86.5	70.8	79.3	86.3	68.2	66.9	50.2	82.4	95.2	68.5	69.1	33.0	85.2	85.4	34.5	35.2	31.4	56.2	67.2	
Sela-v2 [79]	RN-50	80.1	80.4	90.2	89.7	93.3	89.4	89.1	77.1	80.2	94.8	92.8	97.7	98.3	98.9	84.4	82.5	73.3	74.7	98.0	85.7	86.1	89.2	92.9	96.8	38.5	42.2	47.6	71.3	91.7	
upid++ [15, 37]	RN-50	58.4	60.0	78.6	77.2	91.1	81.0	81.6	53.5	58.9	86.1	85.8	95.5	94.3	96.2	68.4	67.1	74.1	82.9	96.4	67.1	67.1	84.2	85.9	92.1	33.6	35.1	49.2	59.8	91.6	
PIRL [15]	RN-50	71.4	71.8	81.9	81.8	91.8	83.6	83.6	61.9	66.4	91.8	90.1	95.5	94.5	97.2	75.4	71.8	65.3	77.6	96.5	78.7	79.4	87.7	88.8	93.9	38.5	37.4	48.6	58.6	91.5	
clusterfit [30]	RN-50	56.2	57.0	72.8	74.0	90.5	78.7	79.7	48.5	55.4	86.5	83.0	92.4	92.2	93.6	77.2	77.0	87.2	87.4	96.0	65.5	71.4	85.1	85.3	91.8	19.9	24.7	42.5	44.7	84.9	
Deepcluster-v2 [28, 29]	RN-50	83.8	84.2	92.0	91.2	93.4	89.8	89.9	76.3	81.3	96.2	96.1	98.5	98.2	98.6	86.2	86.3	72.5	75.6	97.9	88.6	89.2	93.4	95.2	96.9	48.8	57.5	59.1	80.3	92.2	
SwAV [28]	RN-50	82.9	83.5	91.8	91.2	93.4	89.6	90.0	73.4	81.1	96.1	96.1	98.5	98.6	98.8	86.2	86.3	72.5	75.6	97.9	88.6	89.2	93.4	95.2	96.9	48.8	57.5	59.1	80.3	92.2	
SimCLR [14]	RN-50	78.1	77.6	87.9	88.5	92.5	87.9	88.0	75.4	79.6	94.1	91.5	97.6	98.3	99.4	82.2	82.3	61.9	79.3	98.0	83.8	83.0	88.1	92.8	96.1	41.7	39.7	45.1	76.7	90.4	
MoCo v2 [39]	RN-50	80.6	79.3	83.8	89.8	92.3	84.8	85.5	53.0	74.8	96.0	95.5	98.6	97.6	98.7	83.9	82.5	60.1	90.1	96.8	86.8	86.5	95.6	94.6	93.3	45.5	48.4	39.3	74.8	87.5	
SimSiam [74]	RN-50	79.0	79.0	67.0	87.8	89.1	81.8	84.0	24.2	66.5	95.4	94.8	97.8	95.4	98.5	83.9	82.5	60.2	87.0	96.3	87.0	87.0	94.6	97.0	97.3	65.4	49.2	26.0	77.3	65.4	
BYOL [16]	RN-50	82.1	82.3	90.9	90.5	93.0	89.1	89.0	76.4	80.7	95.8	95.1	98.5	98.1	99.0	87.0	84.3	82.1	86.0	98.1	87.8	87.3	93.6	95.4	96.5	62.7	67.2	71.0	84.3	93.5	
Barlow Twins [75]	RN-50	81.1	81.2	89.9	89.4	91.9	87.4	86.5	73.9	76.3	95.9	95.2	98.0	97.6	98.3	85.5	82.9	83.5	83.4	97.7	88.4	88.1	93.8	94.6	95.7	58.4	64.0	71.4	82.2	86.8	
DenseCL [80]	RN-50	72.5	72.8	76.6	85.6	92.0	83.7	84.6	54.6	69.8	95.7	96.2	96.1	97.2	97.6	76.4	77.6	56.9	84.1	96.8	83.4	83.5	76.8	91.2	93.3	35.4	38.1	31.3	61.3	88.6	
DINO [22]	RN-50	83.8	83.4	92.1	91.3	93.3	89.4	89.8	72.9	80.6	96.2	96.0	98.5	98.2	99.0	82.8	81.4	74.8	78.3	98.0	89.5	88.8	93.7	95.2	96.9	48.3	57.0	60.0	67.0	80.4	92.6
MoCo v3 [47]	RN-50	84.2	84.3	88.3	91.8	91.0	93.4	89.7	90.0	77.7	82.5	96.5	95.0	98.4	97.9	98.7	87.5	82.9	85.4	86.9	98.2	89.5	88.0	95.3	95.5	96.7	73.0	74.0	95.0	95.1	96.3
DINO [22]	ViT-B/16	91.1	91.2	93.1	93.6	95.6	92.8	93.7	87.9	90.2	97.5	97.5	99.2	99.1	99.4	94.1	93.7	97.2	97.3	99.0	96.1	96.3	97.5	97.9	98.1	85.7	86.0	95.0	95.1	96.3	
iBOT [17]	ViT-B/16	91.7	91.7	93.8	94.2	96.2	94.0	94.5	89.9	91.8	97.9	98.2	99.2	99.1	99.3	93.7	93.6	97.2	97.3	99.3	96.1	96.4	97.8	98.0	98.4	84.7	85.0	94.9	95.3	96.4	
MoCo v3 [47]	ViT-B/16	88.3	88.7	91.9	93.0	95.5	92.5	92.0	60.2	88.0	96.8	95.7	99.3	98.2	98.3	93.5	93.7	95.1	97.1	98.9	92.8	93.3	93.5	97.2	96.3	72.6	74.0	72.8	91.2	86.9	
MAE [9]	ViT-B/16	44.1	44.6	68.4	86.3	94.6	88.8	89.6	71.3	71.1	89.8	89.2	97.5	97.8	98.6	46.4	47.4	75.4	76.7	90.4	98.2	97.1	90.9	91.2	92.6	95.9	16.4	37.3	20.1	73.9	92.6
MaskFeat [32]	ViT-B/16	26.0	48.9	10.7	75.5	92.6	80.5	86.0	23.7	23.1	71.0	72.5	83.4	52.0	92.7	88.0	56.2	71.5	28.6	85.9	96.7	38.0	51.9	11.7	79.7	89.5	12.7	17.0	6.4	36.6	66.5
BEiT v2 [72]	ViT-B/16	86.9	87.2	94.3	94.1	97.4	95.8	95.0	92.4	97.6	97.9	99.3	99.2	99.3	99.2	99.2	92.2	97.5	97.6	99.1	94.7	41.7	43.2	78.0	80.5	97.1	91.1	92.1	92.0	92.3	92.5
MILAN [35]	ViT-B/16	89.9	90.8	94.2	94.9	97.4	95.5	95.5	90.8	91.8	98.1	98.2	99.5	99.9	99.9	90.3	90.5	92.6	92.6	99.0	96.3	97.1	98.5	99.2	95.0	85.0	85.0	84.6	94.4	96.5	
EVA [34]	ViT-B/16	68.3	72.8	83.1	88.8	96.0	91.2	91.8	70.2	79.3	91.2	93.1	98.4	97.7	99.0	81.8	84.9	83.6	95.4	98.3	74.8	79.5	84.9	94.6	97.1	28.6	32.5	27.2	69.1	89.8	
PixMIM [36]	ViT-B/16	59.4	70.5	81.7	87.0	94.7	86.2	87.6	52.0	71.5	84.9	90.6	93.8	90.0	97.7	71.1	83.0	78.7	93.2	97.2	67.3	80.4	59.1	92.9	94.3	25.7	35.8	23.4	70.9	80.0	

Method	Backbone	Imagenet-D						Cifar100						Caltech-256						CUB												
		Clipart	Infograph	Painting	Quickdraw	Real	Sketch	kNN	kNN ^N	LP	LP ^{BN}	FT	kNN	kNN ^N	LP	LP ^{BN}	FT	kNN	kNN ^N	LP	LP ^{BN}	FT	kNN	kNN ^N	LP	LP ^{BN}	FT					
Jigsaw [48]	RN-50	31.4	32.3	42.1	58.2	83.7	81.2	18.3	22.6	28.1	50.9	28.4	28.1	44.9	55.4	77.5	55.0	56.9	38.4	53.0	92.5	52.9	52.9	69.0	77.0	91.2	28.7	29.6	35.9	48.3	78.1	
rotnet [78]	RN-50	42.0	42.9	56.2	68.3	85.9	81.8	19.3	27.8	33.6	54.2	38.1	37.5	57.4	64.6	74.9	53.9	59.6	52.9	67.8	76.2	76.8	70.6	60.8	76.0	81.8	92.0	38.0	38.7	50.4	61.1	80.2
upid [37]	RN-50	49.0	48.3	22.4	69.0	83.1	72.4	27.7	15.0	35.3	51.2	47.6	47.6	35.7	67.4	77.2	65.6	62.5	24.6	73.2	92.1	74.5	74.5	62.7	84.3	91.2	45.5	44.5	21.9	60.4	77.8	
Sela-v2 [79]	RN-50	55.9	54.5	70.8	76.2	90.0	93.1	32.9	40.7	44.0	61.2	60.0	61.2	77.4	78.9	77.3	55.1	49.1	60.4	71.3	92.2	86.0	86.2	91.3	91.6	94.8	51.4	51.2	65.8	69.8	84.9	
upid++ [15, 37]	RN-50	42.7	40.7	64.6	68.3	86.4	82.7	27.5	34.6	35.0	54.4	45.8	45.3	67.4	66.6	80.1	48.4	37.8	56.8	71.6	92.5	74.3	84.8	85.5	35.3	51.2	55.8	80.5				
PIRL [15]	RN-50	56.2	55.1	70.9	76.5	87.5	80.3	32.1	38.0	41.8	57.0	56.9	56.6	72.5	74.0	80.5</td																

C Additional Visualizations

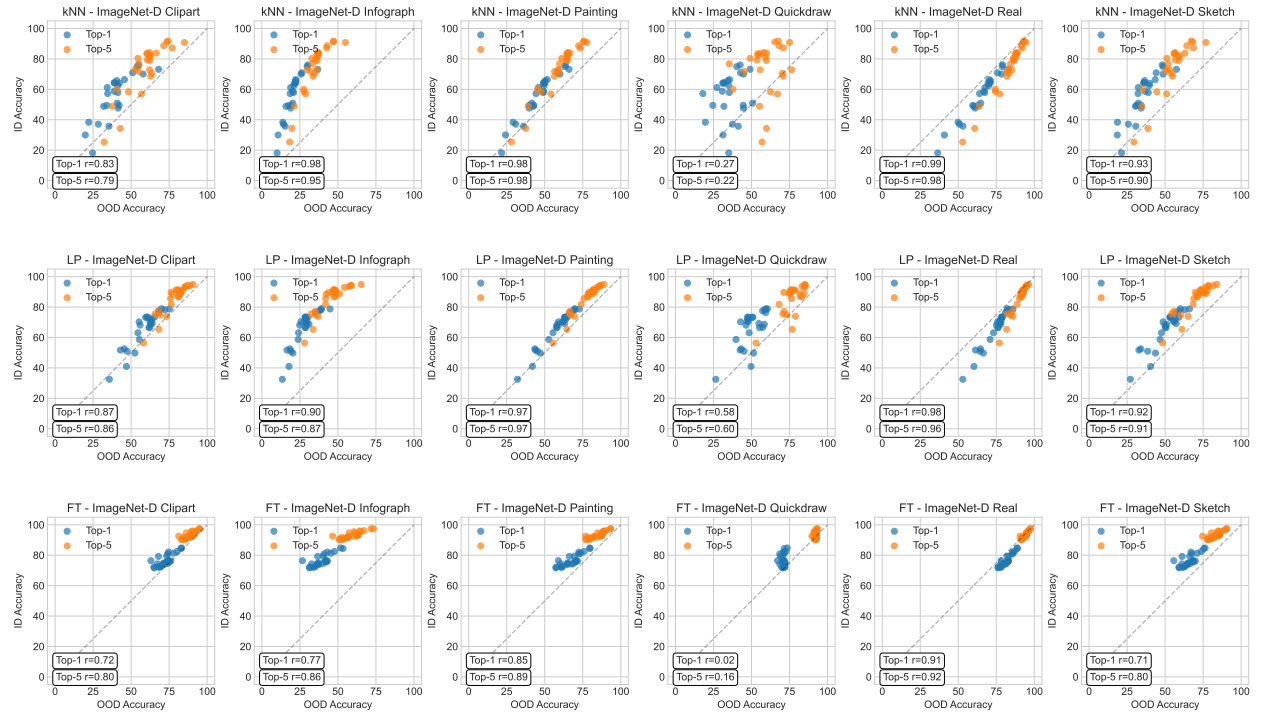


Figure S.1: ImageNet-D ID vs. OOD accuracies on different protocols. We compare both top-1 and top-5 classification accuracies. Correlation coefficients r are calculated using Spearman's rank correlation.

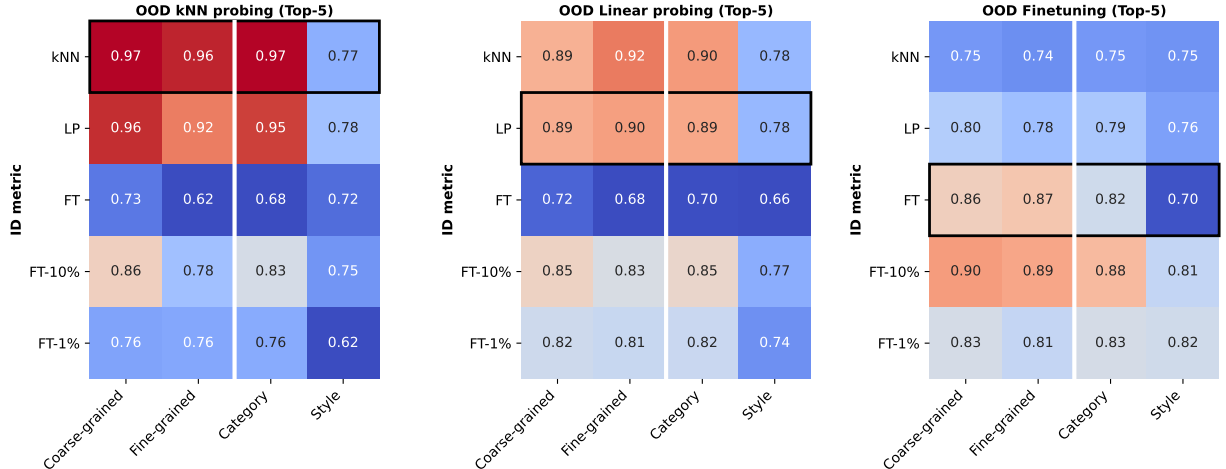


Figure S.2: Spearman rank correlations of top-5 classification accuracies derived from in-domain and out-of-domain protocols under certain types of domain shift. See Fig. 3 for more details.

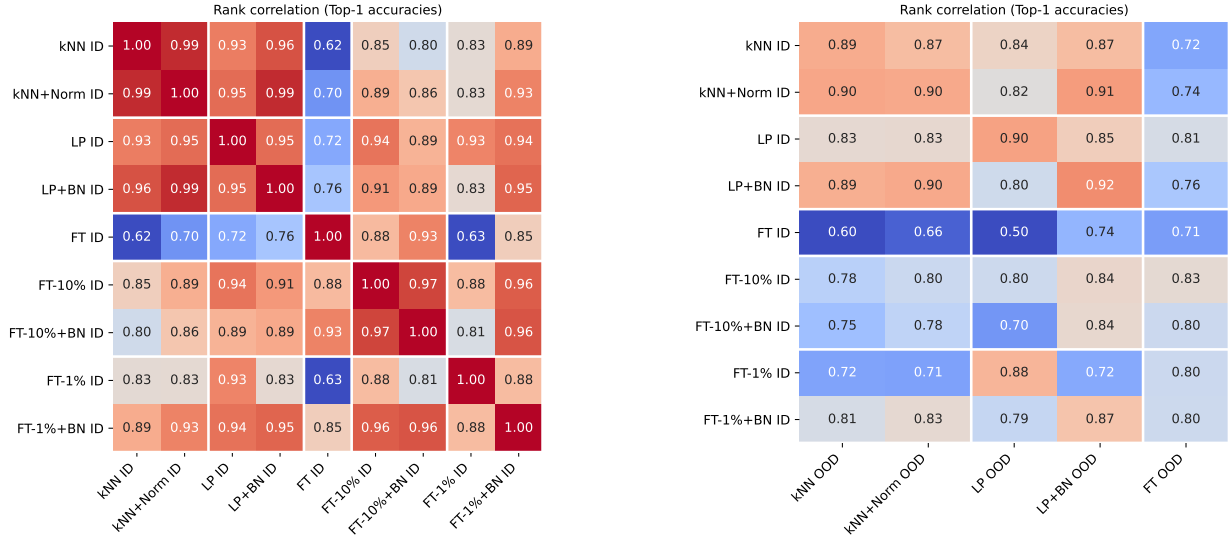


Figure S.3: Extended version of Fig. 2. We show both versions, with and without feature normalization for all protocols but 100% fine-tuning.

D Fine-grained experiments

The iNaturalist data set comes with different levels of hierarchical classes. Taxonomic closeness is a rough proxy for the degree of visual similarity and implies different degrees of fine-graininess of visual features [62]. We use the three most fine-grained targets, “Family”, “Genus”, and “Species” to estimate whether evaluation protocols or models are more or less sensitive to fine-grained features than others. For “Family” we use the full iNat mini data set comprising 1103 classes. By definition, more fine-grained classes would increase the number of classes when the whole dataset is used. To ensure a fair comparison with “Genus” and “Species” targets, we create subsampled datasets that have the same number of classes. At the same time, we ensure that the number of categories higher-level categories for a subset is as small as possible. In detail, we realize this as follows: For the “Genus” subset, we select the 256 families from the “Chordata” phylum that contain the most species, resulting in 1103 “Genus” categories. For the “Species” subset, we sort the previously defined Genus subset by the number of species and pick the top 277 categories, resulting in 1103 “Species” targets.

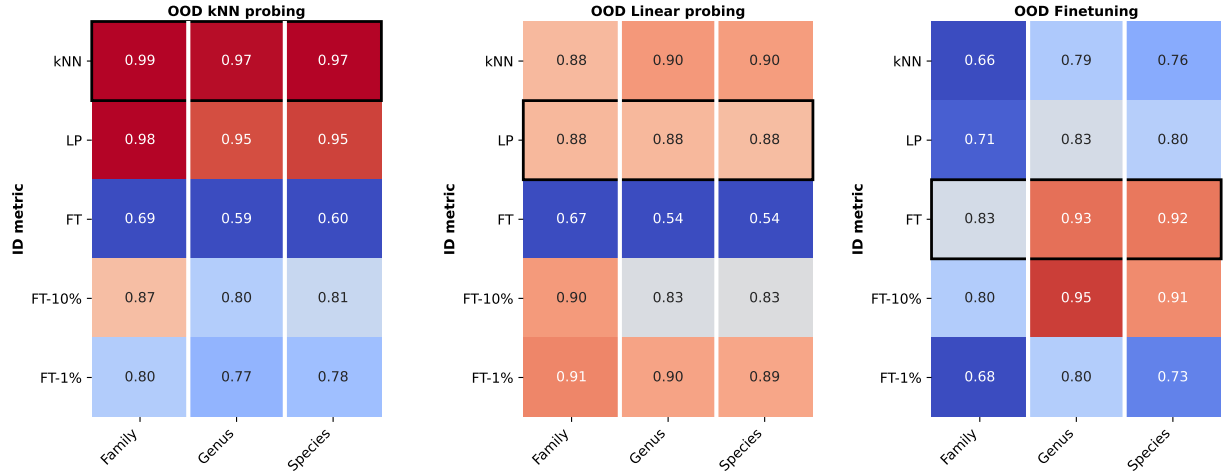


Figure S.4: Spearman rank correlations of top-1 classification accuracies for three different targets in the iNaturalist mini dataset.

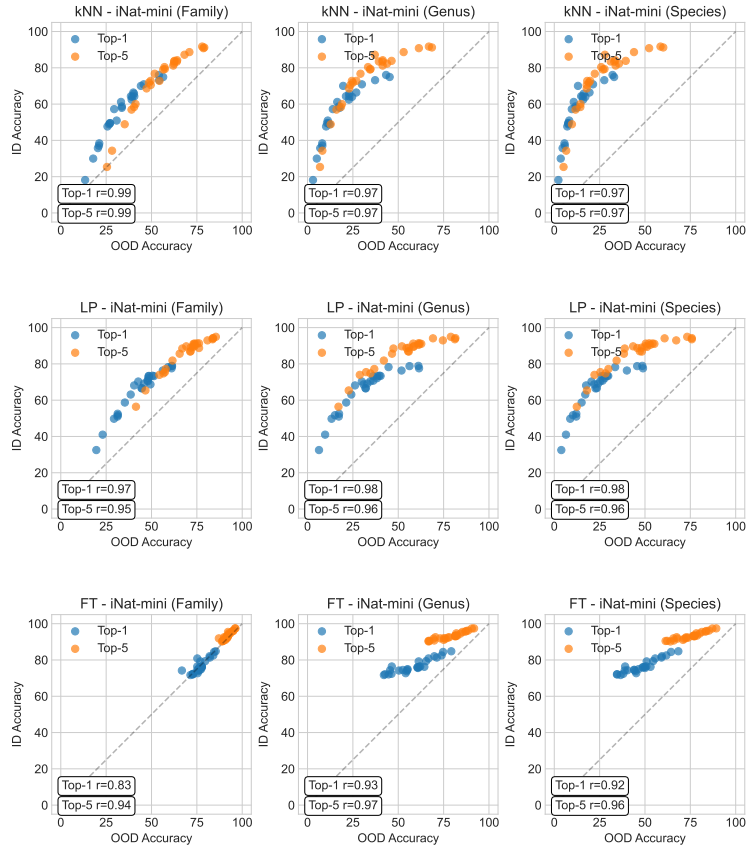


Figure S.5: iNaturalist ID vs. OOD accuracies with different targets (family, genus, species) on different protocols. We compare both top-1 and top-5 classification accuracies. Correlation coefficients r are calculated using Spearman's rank correlation.

E Implementation Details

All experiments were run using models implemented in PyTorch [81] using the `timm` [82] and `mmselfsup` [83] libraries. All end-to-end fine-tuning and linear probing were trained using a Stochastic Gradient Descent optimizer with 100 total epochs (5 warmup epochs followed by Cosine Annealing decay) and a base learning rate of 0.1. Few-shot fine-tuning on ImageNet was trained on 30 epochs only as proposed by [16]. We found this few-shot setup to be the most stable compared to others that have different learning rates for head and backbone (see, e.g., [28, 75]). The effective batch sizes varied per data set and can be found in Tab. S.4. When training vision transformers, we also use layerwise learning rate decay (0.65), label smoothing (0.1), and drop path (0.2), inspired by [9].

Table S.4: Chosen effective batch sizes for different data sets used in this study.

Dataset	End-to-end fine-tuning	linear probe
ImageNet-1k (full)	256	1024
ImageNet-1k (10%)	256	-
ImageNet-1k (1%)	256	-
Pascal VOC	32	32
Caltech-256	32	32
CUB	32	32
Cifar100	128	128
iNaturalist mini, Family	256	1024
iNaturalist mini, Genus	256	1024
iNaturalist mini, Species	256	1024
ImageNet-D Clipart	128	128
ImageNet-D Infograph	128	128
ImageNet-D Painting	128	128
ImageNet-D Quickdraw	256	256
ImageNet-D Real	256	256
ImageNet-D Sketch	128	128

KNN-probing was implemented with `scikit-learn` [84] using Euclidean distance, a brute force solver, and $k = 20$ neighbors (as proposed by [22]).

For ResNet-50, we use the last 2048-dimensional (pre-logit) representation to report probing accuracy. [85] described that this consistently works better for this architecture than using any intermediate latent representation. For Vision Transformers, we follow the protocol of most implementations by training the linear classifier on the 768-dimensional `cls`-token.

Certain models—especially those using masked image modeling — achieve a significantly better linear probe accuracy when batch normalization is used between the model outputs and the linear classifier, as suggested by [9] and verified by [65]. Based on our own experiments, we can see that normalization has either a strong positive or an insignificant effect on the accuracy depending on the model (see Tab. S.2). Accordingly, we decided to use batch normalization for linear probing and also normalize latent representations before kNN probing. Tab. S.5 lists the sources of the pre-trained model checkpoints we used.

Table S.5: Sources of the pre-trained model checkpoints used in this study.

Method	Backbone	Source
Jigsaw	RN-50	VISSL model zoo
rotnet	RN-50	VISSL model zoo
npid	RN-50	VISSL model zoo
Sela-v2	RN-50	SwAV official Github
npid++	RN-50	VISSL model zoo
PIRL	RN-50	VISSL model zoo
clusterfit	RN-50	VISSL model zoo
Deepcluster-v2	RN-50	Deepcluster official Github
SwAV	RN-50	SwAV official Github
SimCLR	RN-50	VISSL model zoo
MoCo v2	RN-50	MoCoV2 official Github
SimSiam	RN-50	MMSelfSup model zoo
BYOL	RN-50	Github (inofficial)
Barlow Twins	RN-50	MMSelfSup model zoo
DenseCL	RN-50	DenseCL official Github
DINO	RN-50	DINO official Github
MoCo v3	RN-50	MoCoV3 official Github
DINO	ViT-B/16	DINO official Github
iBOT	ViT-B/16	iBOT official Github
MoCo v3	ViT-B/16	MoCoV3 official Github
MAE	ViT-B/16	MAE official Github
MaskFeat	ViT-B/16	MMSelfSup model zoo
BEiT v2	ViT-B/16	BEiT official Github
MILAN	ViT-B/16	MILAN official Github
EVA	ViT-B/16	MMSelfSup model zoo
PixMIM	ViT-B/16	MMSelfSup model zoo

Table S.6: Overview of how datasets were categorized in our domain shift experiments (Fig. 3). We define domain shifts w.r.t. ImageNet-1k.

Dataset	Coarse	Fine	Category	Style
Pascal VOC	✓			
Caltech256	✓		✓	
CUB		✓	✓	
iNat mini Family	✓		✓	
iNat mini Genus		✓		
iNat mini Species		✓		
ImageNet-D Clipart				✓
ImageNet-D Infograph				✓
ImageNet-D Painting				✓
ImageNet-D Quickdraw				✓
ImageNet-D Sketch				✓

F Approximating Errors

Running the full set of experiments multiple times is costly. Therefore, we randomly selected one model per metric per dataset and ran the same experiment three times in order to approximate a representative error value (see Tab. S.7). We can see that errors are generally small and conclude that our metrics generated by a single run can be trusted.

Table S.7: Top-1 accuracies for three different seeds of different models on different datasets. Generally, metrics generated by evaluation protocols are highly reproducible. Note that we do not cover the uncertainty introduced by different pre-training setups.

Protocol	Dataset	Method	Backbone	Run 1	Run 2	Run 3	mean	std
Linear Probing	ImageNet	SimCLR	RN-50	66.87	66.82	66.85	66.85	0.02
Fine-tuning	ImageNet	DINO	RN-50	76.00	76.01	76.27	76.09	0.12
10% Fine-tuning	ImageNet	MILAN	ViT-B/16	78.92	78.91	78.91	78.91	0.01
1% Fine-tuning	ImageNet	EVA	ViT-B/16	41.10	46.65	46.65	44.80	2.62
Linear Probe	Pascal VOC	Deepcluster v2	RN-50	85.66	85.72	85.86	85.75	0.08
Fine-tuning	Pascal VOC	Jigsaw	RN-50	64.62	64.73	63.22	64.19	0.69
Linear Probe	Caltech-256	BEiT v2	ViT-B/16	90.22	90.25	90.26	90.24	0.02
Fine-tuning	Caltech-256	MoCo v3	RN-50	88.52	88.53	88.40	88.48	0.06
Linear Probe	CUB	DINO	ViT-B/16	78.17	78.41	78.48	78.35	0.13
Fine-tuning	CUB	SeLa v2	RN-50	68.23	68.93	68.16	68.44	0.35
Linear Probe	iNat mini (family)	SwAV	RN-50	46.94	47.27	47.13	47.11	0.14
Fine-tuning	iNat mini (family)	Barlowtwins	RN-50	66.72	66.71	66.86	66.76	0.07

G Computational Costs of Protocols

Table S.8: Estimated computational cost of different protocols. GPU-based metrics were estimated based on training on 2x NVIDIA RTX A5000. For k-NN, we neglect CPU-based time required by the classifier and only account for GPU-time used for model inference. The values shown are for ImageNet-1k (in-domain) protocols. Hyperparameters for other datasets can be found in Appendix E.

Protocol	Batch size	epochs	GPU hours	
			ResNet-50	ViT-B/16
kNN	1024	-	0.6	1.3
LP	1024	100	36	70
FT	256	100	94	184
10%-FT	128	30	3.5	6.5
1%-FT	128	30	1.0	1.5